1	
2	
3	Multiple Intrinsic Membrane Properties are Modulated in a Switch from Single- to Dual
4	Network Activity
5	
6	Ryan R. Snyder
7	Dawn M. Blitz¹
	Dawn W. Ditz
8	
9	
10	Department of Biology and Center for Neuroscience
11	
12	Miami University
13	Oxford OH 45056
14	
15	Running title: Neuronal switching via modulation of multiple properties
16	
17	¹ Corresponding Author:
18	Dawn M. Blitz
19	700 E High St
20	PSN 212
21	Oxford OH, 45056
22	<u>blitzdm@miamoh.edu</u>
23	513-529-6327
24	
25	ORCiD: 0000-0002-1281-6010
26	

Abstract

27 28

29

30

31

32

33

34

35

36

37

38

39

40

41

42

43

44

45

46

47

48

49

50

Neural network flexibility includes changes in neuronal participation between networks, such as the switching of neurons between single- and dual-network activity. We previously identified a neuron that is recruited to burst in time with an additional network via modulation of its intrinsic membrane properties, instead of being recruited synaptically into the second network. However, the modulated intrinsic properties were not determined. Here, we use small networks in the Jonah crab (Cancer borealis) stomatogastric nervous system (STNS) to examine modulation of intrinsic properties underlying neuropeptide- (Gly¹-SIFamide) elicited neuronal switching. The LPG neuron switches from exclusive participation in the fast pyloric (~1 Hz) network, due to electrical coupling, to dual-network activity which includes periodic escapes from the fast rhythm via intrinsically-generated oscillations at the slower gastric mill network frequency (~0.1 Hz). We isolated LPG from both networks using pharmacology and hyperpolarizing current injection. Gly¹-SIFamide increased LPG intrinsic excitability and rebound from inhibition, and decreased spike frequency adaptation, which can all contribute to intrinsic bursting. Using ion substitution and channel blockers, we found that a hyperpolarization-activated current, a persistent sodium current, and a calcium or calcium-related current(s) appear to be primary contributors to Gly¹-SIFamide-elicited LPG intrinsic bursting. However, this intrinsic bursting was more sensitive to blocking currents when LPG received rhythmic electrical coupling input from the fast network than in the isolated condition. Overall, a switch from single- to dual-network activity can involve modulation of multiple intrinsic properties, while synaptic input from a second network can shape the contributions of these properties.

51 Keywords

- Neuromodulation, central pattern generator, neuronal switching, Stomatogastric,
- 53 neuropeptide

54

55 New and Noteworthy

Neuropeptide-elicited intrinsic bursting was recently determined to switch a neuron from single to dual-network participation. Here we identified multiple intrinsic properties modulated in the dual-network state and candidate ion channels underlying the intrinsic bursting. Bursting at the second network frequency was more sensitive to blocking currents in the dual-network state than when neurons were synaptically isolated from their home network. Thus, synaptic input can shape the contributions of modulated intrinsic properties underlying dual-network activity.

63

Introduction

64 65

66

67

68

69

70

71

72

73

74

75

76

77

78

79

80

81

82

83

84

85

86

87

Flexibility of rhythmic networks enables adaptation to changing internal and external environmental demands. This network plasticity results in multiple versions of rhythmic locomotor, respiratory and chewing behaviors, and different oscillatory patterns contributing to sleep, memory formation, and other cognitive processing (1–6). Network flexibility extends to neuronal switching, in which neurons change their participation between networks, including switching between single- and dual-frequency oscillations (7–12).

Neuronal switching contributes to multifunctional roles for neurons and muscles in a number of behaviors (4, 13, 14). For instance, the same neurons participate in combinations of coughing, gasping, and breathing in rodents and cats, and in multiple feeding-related behaviors in molluscs and crustaceans (6, 9, 11, 15–17). Bifunctional muscles similarly switch their participation between different behaviors, such as abdominal muscles in bats that contribute to respiration and the generation of echolocation signals (18). In other cases, rhythmic networks and behaviors are coactive, and coordinating their activity via switching neurons is functionally important (1, 19). Disrupted coordination can lead to behavioral deficits such as aspirating food when swallowing (5, 20). Despite the importance of coordination between networks, it is not a static parameter. In crustacean feeding networks, temperature and oxygen levels alter coordination between networks (21, 22), and locomotor speed alters coupling ratios between human locomotion and respiration (23). Thus, understanding the mechanisms controlling neuronal switching is important to understand function and dysfunction of multiple related networks.

Although neuronal switching is thought to be prevalent in many regions of vertebrate and invertebrate nervous systems, there are few instances of identified cellular-level mechanisms regulating neuronal participation between networks. In smaller, invertebrate systems the predominant mechanism identified for recruiting a neuron into an additional network, or assembling a novel network from multiple discrete networks, is modulation of synaptic strength (11, 12, 24). In addition to synaptic properties, intrinsic membrane properties controlling neuronal excitability are also important targets of neuromodulators that alter network output (25–27). For instance, modulation of intrinsic membrane properties can "release" neurons from a network (8, 12, 28). More recently, we found that modulation of membrane properties can also recruit a neuron into dual-network activity (7), as suggested in computational studies (24, 29). Large, diffuse networks can make it difficult to examine the cellular-level mechanisms of neuronal switching, and thus most mechanistic information comes from studies in smaller, well-defined neural networks (4, 13, 14).

Feeding-related networks in the STNS of the crab, *Cancer borealis*, provide an exceptional model for examining network plasticity, including neuronal switching. The stomatogastric ganglion (STG) contains approximately 30 neurons comprising two rhythmic networks; the fast pyloric (~1 Hz; food filtering) and slow gastric mill (~0.1 Hz; food chewing) networks (30–32). Modulatory inputs from higher order ganglia modulate the pyloric and gastric mill networks to produce different rhythmic outputs (32, 33). The sensitivity of the *C. borealis* STG networks to many neuromodulators correlates with a varied diet of this species (34–36). Particularly relevant to this study, flexibility of STNS

network output in multiple crab and lobster species includes neuronal switching between pyloric, gastric mill, and swallowing networks (7, 11, 12, 37).

A modulatory projection neuron, modulatory commissural neuron 5 (MCN5), uses the neuropeptide Gly¹-SIFamide to elicit a particular gastric mill motor pattern, including interactions between the pyloric and gastric mill networks that differ from those during activation of other modulatory inputs (7, 37). As part of its actions, MCN5 stimulation, or bath-applied Gly¹-SIFamide, switches the lateral posterior gastric (LPG) neuron from solely being active with the pyloric rhythm, to dual-frequency bursting in time with the pyloric and gastric mill rhythms (7, 37). In C. borealis, LPG typically generates fast (~1 Hz) bursts due to electrical coupling with the other pyloric pacemaker ensemble neurons (7, 37, 38). However, in the MCN5/Gly¹-SIFamide modulatory state, LPG generates pyloric-timed bursts, due to continued electrical coupling to pyloric pacemaker neurons, plus slower, gastric mill-timed bursts that are generated due to Gly¹-SIFamide modulation of LPG intrinsic properties (7, 37). The membrane properties underlying the switch from single to dual-network activity have not been determined (7). Here, we extended our previous study to examine intrinsic properties modulated by Gly¹-SIFamide, and ionic currents contributing to the LPG switching neuron generating intrinsic oscillations at a second frequency.

128

129

130

131

132

110

111

112

113

114

115

116

117

118

119

120

121

122

123

124

125

126

127

Methods

Animals

Male C. borealis crabs were purchased from the Fresh Lobster Company (Gloucester,

MA) and housed in artificial seawater tanks (10-12°C). Immediately prior to dissection,

crabs were anesthetized by packing in ice (45-55 min). Dissections were performed as previously described (7, 39). The foregut was removed from the crab, bisected ventrally, and pinned in a Sylgard (170: Thermo Fisher Scientific, Watham, MA)-coated dissection dish containing chilled (8-10°C) *C. borealis* physiological saline. The STNS was dissected free from muscle and other tissue, transferred to a petri dish and pinned on a layer of clear Sylgard (184; Thermo Fisher Scientific). To optimize our experimental schedule, preparations were stored overnight at 4°C in *C. borealis* physiological saline until used in electrophysiology experiments the following day. Both pyloric and gastric mill rhythms are stable for multiple days in this *in vitro* system (40, 41) and the effects of Gly¹-SIFamide applications do not differ in preparations dissected the same day versus the previous day (S-RH Fahoum and DM Blitz, unpublished).

Solutions

C. borealis physiological saline (pH 7.4 – 7.6) consisted of the following (in mM): 440 NaCl, 26 MgCl₂, 13 CaCl₂, 11 KCl, 10 Trisma base, 5 Maleic acid. For low Ca²⁺ saline, 90% of Ca²⁺ was replaced with equimolar (11.7 mM) MnCl₂. Riluzole (BD Solutions), a persistent sodium current blocker (42), was dissolved in 100% dimethylsulfoxide (DMSO; Thermo Fisher Scientific) at 100 mM and aliquots stored at -20°C. Prior to use, riluzole aliquots were thawed and diluted in *C. borealis* saline (30 μM) such that the final DMSO concentration was less than 1%. At this concentration, DMSO does not affect STG neurons (43–45). Cesium chloride (CsCl; Sigma Aldrich), a hyperpolarization-activated inward current blocker (42, 46, 47), was dissolved in *C. borealis* saline on the day of experiments at a final concentration of 5 mM. Picrotoxin (PTX; Sigma Aldrich)

was dissolved in *C. borealis* saline or low Ca²⁺ saline at 10 μM and mixed thoroughly (> 45 min) immediately prior to use. PTX was used to block inhibitory glutamatergic synapses (7, 48). The neuropeptide Gly¹-SIFamide (GYRKPPFNG-SIFamide, custom peptide synthesis: Genscript) (37) was dissolved in H₂O Optima (10⁻² M) and stored at -20°C. Aliquots were thawed and dissolved directly in the appropriate solution (*C. borealis* saline, 10 μM PTX in *C. borealis* saline or low Ca²⁺ saline, or saline plus CsCl and/or Riluzole) immediately prior to use at a final concentration of 5 μM. Solution changes were controlled by a switching manifold. Squid internal electrode solution consisted of (in mM): 20 NaCl, 15 Na₂SO₄, 10 Hepes, 400 potassium gluconate, 10 MgCl₂ (49).

Electrophysiology

Petroleum jelly (Vaseline; CVS) wells were built around nerves to electrically isolate them from the rest of the bath. Extracellular recordings were obtained using paired stainless-steel electrodes. One electrode from each pair was placed adjacent to the nerve within a petroleum jelly well and the reference electrode from each pair was placed outside the well. Extracellular recordings were amplified with a differential AC amplifier (Model 1700; A-M systems, Sequim, WA).

The STG was desheathed prior to each experiment to facilitate visualizing STG somata for impalement. Intracellular recordings were obtained using pulled-glass sharp microelectrodes (30-50 M Ω) filled with a squid internal electrode solution (see Solutions). Intracellular recordings were amplified with an Axoclamp 900A amplifier (Molecular Devices, San Jose, CA). Intracellular and extracellular signals were digitized

(~5 kHz sampling rate) and recorded to a lab computer (Dell, Round Rock, TX) using data acquisition hardware (Micro1401; Cambridge Electronic Design [CED], Cambridge, U.K.) and software (Spike2; CED). Current injections were performed manually through the Axoclamp 900A commander software or via custom Spike2 stimulus sequence files. Intracellularly recorded neurons were identified by their activity patterns, synaptic input, and by confirming their axonal projection pattern through spike-triggered averaging of neuron and nerve recordings (7, 31, 50). For accurate membrane potential measurements during current injections, some experiments were performed with either two-electrode current clamp (TECC; dual-impalement) or discontinuous current clamp (DCC; single impalement; sampling rate: 5 kHz). For DCC, the electrode time constant was minimized using the internal amplifier capacitance neutralization. In some experiments, electrodes were coated with Sylgard 184 (Fisher Scientific) to reduce electrode capacitance and facilitate DCC (51).

Electrophysiology experiments, unless otherwise specified, were performed in the presence of PTX with both PD neurons hyperpolarized (PTX:PDhype). Each PD neuron was hyperpolarized by negative current injection in single electrode bridge mode using an Axoclamp 900A (Molecular Devices) to eliminate the influence of rhythmic input through electrical synapses between LPG and the AB/PD pyloric pacemaker ensemble (7, 38, 52). Due to the rectification of electrical coupling between PD and LPG, PD hyperpolarization has little effect on the LPG membrane potential (Fahoum and Blitz 2021; Shruti et al. 2014). PTX eliminates the influence of glutamatergic chemical synapses, including the single known chemical synaptic input to LPG, the LP

neuron (7, 48). In a subset of experiments without PTX, hyperpolarizing DC current was injected into the LP neuron (LP_{hype}) to eliminate input from LP to LPG (7).

203

204

205

206

207

208

209

210

211

212

213

214

215

216

217

218

219

220

221

201

202

LPG Burst Detection

To identify LPG bursts, LPG spikes were detected in extracellular nerve (*lpgn*) recordings. For the PTX:PDon condition, a histogram of LPG interspike intervals (ISIs) across Gly¹-SIFamide applications was made for each experiment. Histograms included a cluster of short duration ISIs representing intervals between spikes within a burst and a cluster of longer duration ISIs representing the intervals between bursts. The median of the two ISI distribution peaks was calculated and selected as the maximum interval for two successive spikes to be considered part of the same burst. After calculating an ISI cutoff value, LPG bursts were identified as groups of two or more successive spikes with ISIs shorter than the calculated ISI cutoff (7). LPG slow bursts were then selected by subtracting LPG bursts with a duration shorter than two pyloric cycles (two consecutive PD bursts), using a custom Spike2 script (7). This eliminated the faster, pyloric-timed LPG bursts originating from electrical coupling to the AB/PD neurons (38). All LPG burst analysis in the PTX:PDon condition includes only the slower, intrinsic LPG bursts. For the PTX:PDhype condition a cutoff ISI was used to identify bursts as described for the PTX:PDon condition. However, all LPG bursts during PTX:PDhype were considered to be intrinsically generated and were included in analyses because LPG was isolated from rhythmic synaptic input from both networks.

222

Analysis of Intrinsic Properties

223

224

225

226

227

228

229

230

231

232

233

234

235

236

237

238

239

240

241

242

243

244

Input resistance was calculated from the change in voltage in response to hyperpolarizing current injections (-1 nA; 5 s) from the same membrane potential in PTX:PD_{hype} and 5 µM Gly¹-SIFamide in PTX:PD_{hype}. Sag potential amplitude was measured as the difference between the membrane potential immediately before the end of a hyperpolarizing current injection and the most hyperpolarized membrane potential near the beginning of a hyperpolarizing current injection. In each experiment the current injection amplitude was adjusted in the SIF:PTX:PD_{hype} condition to match the most hyperpolarized membrane potential (± 4.0 mV) reached in the PTX:PD_{hype} condition in response to -1 nA (5 s). The amplitude measured during two current injections per condition, per experiment were averaged. There were no differences in the sag voltage between repeated current injections within a condition (Trial 1 vs 2: PTX:PD_{hype}, p = 0.859; SIF:PTX:PD_{hype}, p=0.639, paired t-test). To quantify postinhibitory rebound, the four second period immediately preceding the same hyperpolarizing current steps used to measure sag was selected as a baseline. This baseline was subtracted from the four second period beginning 200 ms after the termination of the current step, and the integrated area of the LPG membrane potential above baseline was calculated using the Spike2 'Area Under Curve' function (53, 54). Two measurements in the PTX:PD_{hype} condition and in the SIF:PTX:PD_{hype} condition were averaged. There were no differences in the integrated area between repeated trials within a condition (Trial 1 vs 2: PTX:PD_{hype}, p = 0.589; SIF:PTX:PD_{hype}, p=0.183, paired t-test).

Firing frequency (# of spikes – 1 / burst duration) was measured across 5 s depolarizing current steps (0.25 – 3.0 nA). A subset of these current steps was used to quantify spike frequency adaptation (SFA). In each experiment, the smallest current amplitude that elicited spiking across the 5 s duration in the PTX:PDhype condition (1 – 3 nA), and the current amplitude that depolarized LPG to the same membrane potential (± 3.0 mV) in the SIF:PTX:PDhype condition (1 – 2.5 nA) were selected. The difference in the current amplitude necessary to reach the same voltage ranged from 0 to -1 nA. The ISIs across each step were plotted as a function of time and a linear line of best fit was calculated in Excel (Microsoft, Redmond, WA). The slope value of the best fit line was used as a measure of SFA as it represented the rate at which the interval between spikes changed across the current step.

Analysis of Burst Properties

To quantify the influence of ion channel blockers and ion substitution, LPG bursts were analyzed from extracellular recordings. Burst duration (interval from first to last spike within a burst; s), cycle period (interval from first spike in a burst to the first spike in the subsequent burst; s), and interburst interval (IBI; cycle period – burst duration; s) was measured for LPG slow bursts across a 200 s window once Gly¹-SIFamide effects reached a steady-state, (stable effects for at least 200 s), beginning immediately after Gly¹-SIFamide effects reached steady-state. Trough voltage was measured from intracellular recordings as the most hyperpolarized membrane potential (mV).

Statistical Analysis

267

Following quantification, data was evaluated for normality using a Shapiro-Wilk 268 normality test to determine whether a parametric or non-parametric test should be used. 269 For comparisons between two groups, a paired t-test or Wilcoxon signed rank test was 270 used. This analysis was performed to compare sag potential, input resistance, 271 272 integrated area under the curve, and ISI rate of change between PTX:PDhype and SIF:PTX:PD_{hype} conditions. For each category of experiments, a statistical power 273 analysis was performed and a power level ≥ 0.8 was considered sufficient. For some 274 275 data sets, power was below 0.8 (Table 1). In these datasets there was high variability at n values (n = 5 - 8) comparable to other data sets in this study (e.g., Fig. 5, 6) which 276 would require extremely large n values to generate a sufficient power level. Based on 277 visual observation of plots of all individual experiments in these data sets and the large 278 n values that would be required, we decided it was not prudent to pursue these 279 experiments further. A two-factor within-subjects repeated measures (RM) ANOVA was 280 used to measure the effects of current amplitude and Gly¹-SIFamide on LPG firing 281 frequency, followed by Tukey pairwise comparisons at each current level in PTX:PD_{hype} 282 283 versus SIF:PTX:PD_{hype}. For pharmacological blockade studies, LPG activity parameters were compared across three conditions: pre-control (SIF:PTX:PD_{hype}), treatment 284 285 (SIF:PTX:PD_{hype} + blocker), and post-control (SIF:PTX:PD_{hype}). To compare the three 286 conditions, a one-way RM ANOVA was used followed by post-hoc pairwise comparisons where appropriate (Bonferroni t-test). Statistical significance was p < 0.05. 287 288 Statistical analyses were performed using SigmaPlot software (v. 14; Systat Software, 289 San Jose, CA; RRID:SCR 003210) or SAS (v. 9.4; Cary, NC). Excel software was used

to organize data and MATLAB (Mathworks, Natick, MA; RRID:SCR_001622) and
CorelDraw (Corel Corporation, Ontario, CA) were used to generate graphs and figures.
Related scripts and code are available at https://github.com/blitzdm/Snyder_Blitz_2022.

Results

294

295

296

297

298

299

300

301

302

303

304

305

306

307

308

309

310

311

312

313

314

315

316

317

Modulator-activated Intrinsic LPG Bursting

To examine intrinsic properties and mechanisms of burst generation, we isolated LPG neurons from rhythmic input from the pyloric and gastric mill networks. Picrotoxin (PTX, 10 µM) blocks glutamatergic inhibition (48, 55, 56), including the only chemical synapse onto LPG from other pyloric neurons. In Saline:PTX, LPG continues to produce pylorictimed oscillations due to electrical coupling with the AB/PD neurons (Fig. 1B-C) (52, 57). When Gly¹-SIFamide (5 μM) is applied in the presence of PTX (SIF:PTX), LPG generates dual-network activity including faster, shorter duration bursts in time with the pyloric rhythm (Fig. 1D, red boxes), and slower, longer duration gastric-mill timed bursts (Fig. 1D, blue box). Although the gastric mill-timed LPG bursting occurs via intrinsic mechanisms (7), LPG may receive synaptic input from other gastric mill neurons in order to coordinate their activity (S-RH Fahoum, DM Blitz, unpublished). Any such influence was removed in these experiments via PTX, as PTX also blocks potential chemical synaptic input from other gastric mill neurons (7, 31). To block the influence of rhythmic pyloric input, the two PD neurons were hyperpolarized sufficiently to eliminate rhythmic bursting in the pyloric pacemaker (AB) neuron (7, 57, 58) (see Methods). Hyperpolarizing the PD neurons does not eliminate LPG slow intrinsic bursting due to the rectifying nature of the electrical coupling between PD and LPG (Fig. 1B) (7, 38). Thus, in this isolated condition without rhythmic input from either circuit, Gly¹-SIFamide (SIF:PTX:PD_{hype}) elicits intrinsic bursting at a slow, gastric mill frequency (~ 0.06 Hz) (Fig. 1E) (7). The two baseline conditions used throughout this study were PTX:PDon to examine dual-frequency bursting (e.g., Fig. 1D) and PTX:PDhype to examine isolated slow bursting (e.g., Fig. 1E).

319

320

321

322

323

324

325

326

327

328

329

330

331

332

333

334

335

336

337

338

339

340

Intrinsic Excitability

As an initial measure of LPG excitability, we examined LPG input resistance (R_i) near its resting potential. Injecting negative current (-1 nA; 5 s) in the PTX:PD_{hype} condition hyperpolarized LPG for the duration of the current step (Fig. 2A; grey trace). In the presence of Gly¹-SIFamide (5 µM), an equivalent current step from the same initial membrane potential brought LPG to a more hyperpolarized potential (Fig. 2A; black trace), indicating an increased input resistance in Gly¹-SIFamide (5 µM; SIF:PTX:PD_{hype}) compared to PTX:PD_{hype} alone (Fig. 2A-B; initial V_m: PTX:PD_{hype}, -48.9 $\pm 2.0 \text{ mV}$; SIF:PTX:PD_{hype}, -48.7 $\pm 1.9 \text{ mV}$; R_i: PTX:PD_{hype}, 19.2 $\pm 2.1 \text{ M}\Omega$; SIF:PTX:PD_{hype}, 22.6 \pm 2.4 M Ω ; n = 11; $t_{(10)}$ = 4.462, p = 0.0012, paired t-test). Thus, Gly¹-SIFamide modulation increased the input resistance of LPG near -50 mV. indicating increased excitability within the voltage range of its typical pyloric oscillations. To further examine excitability across a larger range of voltages, the LPG firing frequency was measured before and during Gly¹-SIFamide application in response to depolarizing current steps (0.25 – 3 nA; 5 s) from the same membrane potential (± 3.0 mV). In an example experiment, in the PTX:PD_{hype} condition, a depolarizing current step (0.5 nA; 5 s) evoked a relatively low firing frequency (7 Hz) (Fig. 2Ci), while 1.5 and 2.5 nA elicited higher firing rates (18 and 22 Hz) (Fig. 2Cii, Ciii). In the presence of Gly¹-

was altered by Gly¹-SIFamide, as a function of current step amplitude (Fig. 2E)

SIFamide, the same amplitude current injections elicited higher firing frequencies (15,

25, 26 Hz; Fig. 2Di-Diii). Across experiments, the frequency/current (F/I) relationship

2.999, p = 0.016, Two Way RM ANOVA). Specifically, although there was no difference in firing frequency at 0.25 nA ($t_{(6.99)}$ = -1.83; p = 0.109, Tukey post-hoc comparison) the firing frequency was higher in Gly¹-SlFamide compared to PTX:PD_{hype} in response to current steps from 0.5 to 3 nA (**0.5 nA**, $t_{(6.41)}$ = -3.49, p = 0.012; **1.0 nA**, $t_{(6.41)}$ = -4.17, p=0.005; **1.5 nA**, $t_{(6.57)}$ = -3.46, p = 0.012; **2.0 nA**, $t_{(6.41)}$ = -3.45, p = 0.012; **2.5 nA**, $t_{(6.75)}$ = -2.89, p = 0.024; **3.0 nA**: $t_{(8.66)}$ = -2.66, p = 0.027; n = 4 – 10). The positive shift in the LPG F/I relationship indicates that LPG excitability was increased by Gly¹-SlFamide within its typical membrane potential range during an ongoing pyloric rhythm.

Intrinsic Membrane Properties

During the current injections used to assess the LPG F/I relationship, we noted that firing frequency appeared to wane across 5 s current steps (e.g., Fig. 2Ci). Thus, we examined the property of spike frequency adaptation (SFA), in which the interspike interval progressively increases in duration across a period of activity (59–61). To test SFA in LPG, we used current steps (1 – 2.5 nA, 5 s) that depolarized LPG to the same membrane potential before and during Gly¹-SIFamide application (PTX:PDhype, -31.7 ± 2.3 mV; SIF:PTX:PDhype, -29.5 ± 2.0 mV). In the PTX:PDhype condition a depolarizing current step (1 nA; 5 s) elicited an initial LPG firing frequency of ~ 22 Hz (initial 0.5 s; Fig. 3A, Ai) which decayed to ~ 8 Hz (final 0.5 s; Fig. 3A, Aii). When LPG was depolarized to the same membrane potential in Gly¹-SIFamide, the initial LPG firing frequency (initial 0.5 s, ~24 Hz; Fig. 3B, Bi) was similar to PTX:PDhype. However, the firing frequency did not decay to the same extent (final 0.5 s, ~14 Hz; Fig. 3B, Bii) as it did in the control PTX:PDhype condition. To quantify the change in firing frequency, we

plotted the interspike interval (ISI) as a function of time in PTX:PD_{hype} (open circles) and PTX:PD_{hype} plus Gly¹-SIFamide (filled circles) (Fig. 3C) and fit each data set with a line of best fit. In this example experiment, the slope of the line of best fit was steeper in PTX:PD_{hype}, indicating a greater amount of SFA in this control condition compared to Gly¹-SIFamide application (Fig. 3C; Slope: PTX:PD_{hype}, 0.0093; SIF:PTX:PD_{hype}, 0.0036). ISIs were plotted in this manner for each experiment and the slopes of the fit lines were used to compare SFA between conditions. As plotted in figure 3D, the ISI/time slope was steeper in PTX:PD_{hype} versus SIF:PTX:PD_{hype} (Slope: PTX:PD_{hype}, 0.013 \pm 0.002; SIF:PTX:PD_{hype}, 0.005 \pm 0.001; n = 9; Z = -2.666, p = 0.004, Wilcoxon signed-rank) (Fig. 3D). Thus Gly¹-SIFamide decreased the extent of SFA in LPG, which can delay burst termination (59, 62).

As plateau properties can contribute to the active phase of bursting (62, 63), we asked whether LPG expresses plateau potentials. We tested for plateau potentials using brief (10 – 200 ms) depolarizing (1 – 10 nA) current injections. Starting at membrane potentials between -45 and -60 mV, these brief depolarizing steps did not elicit plateau potentials in control PTX:PDhype conditions or during Gly¹-SIFamide (5 μ M in PTX:PDhype) application (n = 6; data not shown). Additionally, if plateau properties contributed to slow bursts, brief hyperpolarizing current injections of sufficient amplitude should prematurely terminate these bursts. However, hyperpolarizing current injections (10 – 200 ms) across a range of amplitudes (-1 to -10 nA), did not terminate Gly¹-SIFamide-elicited bursting in PTX:PDhype (n = 6; data not shown).

Another intrinsic membrane property that often contributes to oscillatory activity in many neuron types is post-inhibitory rebound (PIR), in which a period of inhibition

triggers a more depolarized membrane potential, often with increased activity, compared to pre-inhibition (53, 54, 62, 64). In control conditions (PTX:PD_{hype}), following a negative current step (-1 nA; 5 s; trough V_m: -66 mV) the LPG membrane potential depolarized above the baseline potential (grey dashed line), and fired several (12) action potentials before returning to baseline in the example shown (Fig. 4Ai). This rebound response indicates that LPG expressed PIR in the control condition. After being hyperpolarized to a comparable membrane potential (trough V_m: -67 mV; -1 nA; 5 s) in Gly¹-SIFamide, the LPG membrane potential depolarized to a greater extent and LPG fired more action potentials (61; Fig. 4Aii) compared to PTX:PDhype, suggesting that PIR is modulated by Gly¹-SIFamide. To quantify PIR, we measured the integrated area under the LPG membrane potential during a 4 s window after the end of the current step (Fig. 4Ai-Aii; shaded area; see Methods). The integrated area was greater in Gly¹-SIFamide (20.5 \pm 3.0 mV*ms) compared to PTX:PD_{hype} (4.1 \pm 1.0 mV*ms; n = 8; paired t-test, $t_{(7)} = -6.356$, p = 0.00038) (Fig. 4B). Additionally, more action potentials were elicited in the same 4 s window post-hyperpolarization in SIF:PTX:PD_{hype} compared to the PTX:PD_{hype} control (PTX:PD_{hype}: 2.44 ± 1.44 spikes; SIF:PTX:PD_{hype} 26.38 \pm 6.77 spikes; n = 8; paired *t*-test, $t_{(7)}$ = -4.115, p = 0.004) (Fig. 4C), although there was no difference in the timing of the first action potential post-hyperpolarization $(PTX:PD_{hype}: 0.87 \pm 0.38 \text{ s}; SIF:PTX:PD_{hype}: 0.93 \pm 1.02 \text{ s}; p=0.0554, paired t-test).$ There are multiple ionic currents that can contribute to PIR, including the

387

388

389

390

391

392

393

394

395

396

397

398

399

400

401

402

403

404

405

406

407

408

409

There are multiple ionic currents that can contribute to PIR, including the hyperpolarization-activated inward current, I_h (46, 62, 64, 65). A depolarizing sag in membrane potential during maintained hyperpolarization suggests the activation of I_h.

To assess whether I_h might contribute to PIR, including the larger PIR in Gly¹-SIFamide,

we measured the change in membrane potential from the most hyperpolarized level (dotted lines; Fig. 4Ai-Aii) to the voltage at the end of the step ("sag": brackets, Fig. 4Ai-Aii) during 5 s current steps. LPG was hyperpolarized to a comparable membrane potential (\pm 4 mV; see Methods) in PTX:PDhype and SIF:PTX:PDhype in each preparation. The amplitude of the hyperpolarization-activated sag was larger in Gly¹-SIFamide (Fig. 4D; PTX:PDhype: 1.58 \pm 0.31 mV; SIF:PTX:PDhype: 5.06 \pm 0.85 mV; paired *t*-test, n = 8; $t_{(7)}$ = -5.074, p = 0.00144). These data implicate a hyperpolarization-activated inward current as a contributor to PIR in LPG and a target for Gly¹-SIFamide modulation. To further examine contributions of ionic currents to the intrinsic, slow LPG bursting, we used blockers and ion-substitution in both the isolated (PTX:PDhype), and dual-network (PTX:PDon) conditions.

Ionic Current Contributions

The I_h current is a common target of neuromodulation (65–67). As I_h was implicated in PIR in LPG due to the enhanced sag potential during hyperpolarizing pulses, we assessed a role of I_h in LPG intrinsic bursting by blocking this current using extracellular cesium (5 mM CsCl) (42, 46, 47) (Fig. 5). When Gly¹-SIFamide was bath-applied in CsCl:PTX:PD_{hype}, LPG generated intrinsic bursts, suggesting that the I_h current is not necessary for intrinsic bursting (Fig. 5Aii). However, there were differences in Gly¹-SIFamide-elicited bursts in CsCl compared to the control condition (SIF:PTX:PD_{hype}). Although four bursts were generated during Gly¹-SIFamide in the absence (Fig. 5Ai) or presence (Fig. 5Aii) of CsCl, the cycle period was longer in CsCl in the example shown, with a notable change in the interburst interval (Fig. 5Ai-Aii, black bars denote duration

of first interburst interval in PTX:PDhype). Plotting the average cycle period (Fig. 5B), interburst interval (Fig. 5C) and burst duration (Fig. 5D) with the same y-axis scaling, an increased cycle period in CsCl appeared to be due entirely to an increased interval between bursts. CsCl altered LPG slow burst cycle period (One way RM ANOVA, $F_{(5,2)} = 7.749$, p = 0.009, n = 6) and interburst interval (One way RM ANOVA, $F_{(5,2)} = 20.688$, p < 0.001, n = 6), but did not change burst duration (One way RM ANOVA, $F_{(5,2)} = 0.143$, p = 0.868, p

In control conditions, LPG must escape from the fast (~1 Hz) pyloric-timed input to generate slow, intrinsic bursts. Generating a slow burst despite this rhythmic electrical coupling may have a different dependence on ionic currents compared to the isolated bursting examined above. We therefore tested the role of I_h in LPG slow bursting when it was receiving pyloric input (PTX:PD_{on}). With an ongoing pyloric rhythm (*pdn*), LPG generated dual-frequency bursting in Gly¹-SIFamide in a control SIF:PTX:PD_{on} condition (Fig. 5Ei), as well as in the presence of CsCl (5 μM) (Fig. 5Eii). Blocking I_h with the pyloric rhythm active also extended the Gly¹-SIFamide-elicited LPG slow burst cycle period (Fig. 5E). Similar to the isolated LPG bursting, LPG slow bursts

in the dual-frequency condition appeared to have longer cycle periods (Fig. 5F) that were primarily due to extended interburst intervals (Fig. 5E,G) and not due to a change in burst duration (Fig. 5H), evident in plots of all individual experiments with the same yscaling for the three burst parameters (Fig. 5F-H). In the dual-frequency condition, CsCl changed LPG slow burst cycle period (One way RM ANOVA, F_(7,2) = 6.757, p = 0.009, n = 8), interburst interval (One way RM ANOVA, $F_{(7.2)}$ = 13.386, p < 0.001, n = 8), but did not alter burst duration (One way RM ANOVA, $F_{(7,2)} = 0.809$, p = 0.464, n = 8). Specifically, the cycle period was longer in CsCl + SIF:PTX:PDon compared to SIF-Pre and SIF-Post (Fig. 5F; n = 8; p < 0.05, Table 1) and the interburst interval was longer in CsCl + SIF:PTX:PDon compared to SIF:PTX:PDon before and after the CsCl application (SIF-Pre and SIF-Post; Fig. 5G; n = 8; p < 0.001, Table 1). Thus, in both isolated LPG slow bursting and dual-frequency bursting, blocking In extended the interburst interval without a consistent effect on burst duration, but did not prevent slow bursting. These data suggest that I_h, and likely PIR, contribute to initiating slow bursts, since blocking I_h delayed burst onset.

456

457

458

459

460

461

462

463

464

465

466

467

468

469

470

471

472

473

474

475

476

477

Once a burst is initiated, the inward persistent sodium current (I_{NaP}) can help maintain a depolarized state to prolong burst duration (42, 68, 69). I_{NaP} is present in cultured spiny lobster (*Panulirus interruptus*) stomatogastric neurons, and contributes to LPG slow bursts elicited in response to synaptic input (68, 70). In *P. interruptus*, the LPG neuron is solely active in the slower gastric mill rhythm and is not electrically coupled to the pyloric pacemaker neurons (31, 68). Whether a persistent sodium current contributes to LPG activity in *C. borealis* is unknown. Therefore, we asked whether the

 I_{NaP} blocker riluzole (30 μ M) (42, 71) alters Gly^1 -SIFamide-elicited slow LPG intrinsic bursting.

478

479

480

481

482

483

484

485

486

487

488

489

490

491

492

493

494

495

496

497

498

499

LPG generated intrinsic bursts in Gly¹-SIFamide in riluzole, but the bursts had a shorter cycle period compared to Gly¹-SIFamide alone (Fig. 6Ai-ii). Unlike the effects of CsCl on LPG slow bursting, riluzole decreased LPG cycle period (Fig. 6B; One way RM ANOVA, $F_{(5,2)} = 12.268$, p = 0.004; n = 4 - 6), primarily through a decreased burst duration (Fig. 6D; One way RM ANOVA, $F_{(5,2)} = 23.698$, p < 0.001; n = 4 – 6), with no consistent effect on interburst interval (Fig. 6C; One way RM ANOVA, $F_{(5,2)} = 1.834$, p = 0.221; n = 4 - 6). At ~ 40 min post-riluzole, although there was some return toward control, the effects were still different from control suggesting an incomplete washout (Table 1; Fig. 6B-D). An incomplete riluzole washout, and not a run-down in the LPG response to Gly¹-SIFamide, is likely as the peptide-elicited LPG burst parameters were similar before and after a CsCl application (Fig. 5B-D, F-H). The riluzole and CsCl experiments followed the same time course for the multiple Gly¹-SIFamide applications. Moreover, repeated Gly¹-SIFamide applications in the same preparation without ion channel blockers do not result in a run-down of the LPG bursting (S-RH Fahoum and DM Blitz, unpublished). Overall, INAP was not necessary for isolated LPG slow bursting, but appeared to contribute to the active phase of this bursting in the isolated condition. This contrasts with our findings that blocking In impacted interburst interval but not burst period, suggesting that cycle period may be regulated by a balance between I_h and I_{NaP}. However, we found a different sensitivity of slow LPG bursting to blockade of I_{NaP} when LPG was also expressing fast pyloric bursting.

When Gly¹-SIFamide was applied in in the PTX:PD₀n condition, LPG generated dual frequency bursts in both pyloric and gastric mill time (Fig. 6Ei). With riluzole (30 µM) added, Gly¹-SIFamide produced variable effects on the pyloric rhythm in the PTX:PDon condition. Specifically, in 3/6 preparations, the PD neurons failed to maintain rhythmic bursting in riluzole plus Gly¹-SIFamide. In the 3/6 preparations in which fast rhythmic PD activity persisted, LPG failed to escape the pyloric rhythm and generate slow bursts at steady-state in 2/3 preparations (e.g., Fig. 6Eii). In the remaining one preparation in which the pyloric rhythm remained active in SIF:PTX:PDon + riluzole (30 μM), LPG generated only 8 slow bursts during a 200 s window of steady-state Gly¹-SIFamide application. For comparison, in the control SIF:PTX:PDon condition, there were 18.7 ± 5.0 bursts (n = 3) during a 200 s window of steady-state Gly¹-SIFamide actions. As LPG only produced a few slow bursts in only one experiment, we did not quantify these burst parameters. Two additional experiments were performed in the absence of PTX in which hyperpolarizing current was used to silence the LP neuron and remove chemical synaptic inhibition to LPG (LPhype) as an alternative to PTX (7). In the LP_{hype} experiments, LPG produced only one slow burst (n = 1/2) or entirely failed to escape the pyloric rhythm and generate intrinsic slow bursts at steady state (n = 1/2) during riluzole plus Gly¹-SIFamide application. In summary, in 3/5 preparations in which the pyloric rhythm remained active (2/3 PTX:PDon; 1/2 LPhype), riluzole prevented LPG from escaping rhythmic pyloric input to generate slower intrinsic bursts. In the remaining two experiments, LPG generated only 1 or 8 bursts across a 200 s window. Thus, unlike the isolated LPG neuron, in which I_{NaP} is important for burst duration, but is not

500

501

502

503

504

505

506

507

508

509

510

511

512

513

514

515

516

517

518

519

520

521

essential, when LPG is receiving fast rhythmic input through electrical synapses, I_{NaP} is extremely important for burst occurrence.

Given the complementary actions of I_h and I_{NaP} on interburst interval and burst duration, respectively, we next asked whether co-applying their blockers was enough to eliminate intrinsic LPG bursting. In the PTX:PD_{hype} condition, application of Gly¹-SIFamide elicited intrinsic bursting in LPG (Fig. 7Ai). When Gly¹-SIFamide was applied in the presence of CsCl and riluzole to block both I_h and I_{NaP}, LPG was still able to generate intrinsic bursts (n = 4) (Fig. 7Aii). The riluzole/CsCl combination caused two changes in the LPG slow bursts, an increased interburst interval and a decreased burst duration (Fig. 7), similar to the individual effects of CsCl and riluzole, respectively. However, the persisting ability of LPG to generate slow bursts in the presence of these two blockers, indicated that an additional current(s) is sufficient for intrinsic LPG bursting, at least in the isolated SIF:PTX:PD_{hype} condition.

Although Gly¹-SIFamide decreased the extent of SFA in LPG, there was still some SFA in the modulated condition (Fig. 3). A common mechanism for SFA is the activation of outward I_{KCa} currents during sustained activity. Thus, we next assessed the role of calcium-related currents in LPG intrinsic bursting as currents such as I_{KCa} and I_{CAN} can contribute to intrinsic bursting in many cells (72–76). To test for a role of Ca²+-related currents, we used a low Ca²+ saline with a maintained divalent cation concentration (low Ca²+; 0.1x [Ca²+]; Mn²+ substitution) to decrease calcium influx. This saline decreases calcium influx sufficiently to block transmitter release and outward Ca²+-sensitive currents such as I_{KCa} currents in the STNS (77–82).

Low Ca²⁺ in the SIF:PTX:PD_{hype} condition failed to completely abolish isolated LPG slow bursting. Instead, Gly¹-SIFamide in low Ca²⁺ saline elicited a series of progressively weaker intrinsic LPG bursts (n = 4) coincident with an increasingly depolarized trough membrane potential, eventually devolving into a semi-tonic firing at steady-state (Fig. 8A). Expanded sections of the LPG recording in figure 8A at onset of Gly¹-SIFamide actions (Fig. 8Ai, *left*) and at steady-state (Fig. 8Ai, *right*), better illustrate the depolarized trough potential and the weakened bursting. In the same experiment, the trough voltage remained stable from onset to steady-state in the control SIF:PTX:PD_{hype} condition (Fig. 8B). Across three experiments with an intracellular LPG recording, there was a larger difference in the LPG trough membrane potential between onset and steady-state in Gly¹-SIFamide in low Ca²⁺ compared to SIF:PTX:PD_{hype} (steady-state trough voltage – onset trough voltage in SIF vs. lowCa:SIF; Experiment 1: 0.0 vs. 5.1 mV; Experiment 2: 3.4 vs. 4.2 mV; Experiment 3: 0.0 vs. 14.0 mV). These data suggest that one or more calcium or calcium-related currents are necessary to hyperpolarize the membrane between bursts to activate the hyperpolarization-activated current(s) required for initiating subsequent bursts, and possibly de-inactivate inward currents contributing to burst strength. To determine whether calcium-related currents make similar contributions to LPG

544

545

546

547

548

549

550

551

552

553

554

555

556

557

558

559

560

561

562

563

564

565

566

To determine whether calcium-related currents make similar contributions to LPG slow bursting in the dual-bursting condition, we assessed Gly¹-SIFamide actions in low Ca²+ saline in the PTX:PDon condition. In an example experiment, LPG generated a series of pyloric-timed bursts during onset of Gly¹-SIFamide effects (Fig. 9A, Ai). Throughout the application, the LPG interburst membrane potential progressively depolarized until reaching a steady-state with spike inactivation during bursts (Fig. 9A,

Ai). Although there were several longer duration LPG bursts (2.4 - 2.9 s; Fig. 9A), they coincided with prolonged PD bursts (Fig. 9A, red boxes). Expanded sections of the LPG recording in figure 9A highlight the depolarization of the LPG trough voltage from onset (Fig. 9Ai, *left*) to steady-state (Fig. 9Ai, *right*) Gly¹-SIFamide in low Ca²⁺ saline effects. The trough membrane potential was consistently more depolarized at steady state compared to at the onset of Gly¹-SIFamide in low Ca²⁺ saline (onset: -54.8 \pm 0.9; steady-state: -44.4 \pm 1.5 mV; paired *t*-test, $t_{(5)}$ = -9.365, p = 0.0002, n = 6). The progressive depolarization of trough voltage did not occur in the control SIF:PTX:PDon application (Fig. 9B) (onset: -54.3 \pm 1.5; steady-state: -52.1 \pm 1.5 mV; paired t-test, $t_{(5)}$ = -1.919, p = 0.113, n = 6). The depolarized trough voltage during Gly^1 -SIFamide in low Ca²⁺ saline was similar to that occurring in the isolated LPG bursting in the low Ca²⁺ SIF:PTX:PD_{hype} condition (Fig. 8). However, there was a greater impact of low Ca²⁺ saline on LPG slow bursting when the faster pyloric oscillations were present. Specifically, in 7/11 experiments where rhythmic PD activity persisted in low Ca²⁺ saline plus Gly¹-SIFamide, LPG failed to escape from the faster pyloric input and produce any slow, intrinsic bursts. In the other 4/11 experiments, LPG escaped the pyloric rhythm to produce 1-3 slow, intrinsic bursts during the onset of Gly¹-SIFamide effects in low Ca²⁺ saline before bursting stopped and LPG became either silent or tonic during steadystate. Together, these findings suggest that one or more calcium or calcium-related currents are necessary for periodic escapes from the pyloric rhythm, and further support that calcium-related current(s) are necessary for burst termination and hyperpolarization between bursts.

589

567

568

569

570

571

572

573

574

575

576

577

578

579

580

581

582

583

584

585

586

587

588

Discussion

Previously, we identified a modulatory input and its neuropeptide transmitter that switch a neuron from fast only to dual fast/slow frequency oscillations (7, 37). While the fast oscillations are due to electrical coupling among the fast network pacemaker neurons, the slow oscillations are due to intrinsic properties of the switching neuron and are not dependent upon synaptic input from the second network (7). In this study, we identified multiple intrinsic properties that are modulated by the neuropeptide Gly¹-SIFamide, and several candidate ionic currents that could contribute to the intrinsic bursting.

Furthermore, the sensitivity of LPG slow bursting to blocking currents differed when isolated from both networks versus the dual-frequency condition. This suggests important interactions between electrical coupling input and intrinsic currents in a switching neuron.

Neuronal Switching

Neuromodulators can induce neurons to alter their network participation in invertebrate and vertebrate neural networks (4, 8, 14, 83–86). Neuronal switching includes a neuron changing participation from one network to another, switching between single- and dual-network participation, or reconfiguration of neurons from multiple networks into a novel network (9, 11, 14, 84, 87). Thus far, the mechanisms by which a neuromodulator elicits neuronal switching are mostly identified in smaller invertebrate networks. In general, neuromodulators alter synaptic and/or intrinsic membrane properties of network neurons (25–27). However, the most well-established cellular mechanism for a neuromodulator to elicit a switch in participation is modification of synaptic strength (11,

12, 87). More recent studies highlight an alternate possibility where modulation of intrinsic properties can underlie neuronal participation (7, 8, 29). For example, in large mammalian respiratory networks, modulation of intrinsic properties releases neurons from dual-network participation, although modulation of electrical synapses remains a potential mechanism (8). Further, in the small STNS feeding networks, we found that neuronally-released, or bath-applied neuropeptide Gly¹-SIFamide enables oscillations at a second frequency selectively through modulation of intrinsic properties (7). However, the ion channel targets and intrinsic membrane properties that are altered by this modulatory pathway were not identified. In a computational study, modulation of a slow conductance determined whether a hub neuron participated in single- versus dual-network activity, but these findings were not tested in a biological system (29).

Modulation of Intrinsic Properties

Intrinsic oscillations occur due to a combination of voltage-gated ionic currents contributing to different components of the oscillation. The ability to generate intrinsic oscillations can be enabled or disabled by neuromodulators which alter these ion channel properties (88–91). Different ion channels, or combinations of channels, underlie other intrinsic properties within neurons which may contribute to intrinsic oscillations, or further shape neuronal activity. For instance, in many CPG and other rhythmic networks, inhibition can activate, or de-inactivate voltage-gated currents which in turn drive the active phase of bursting (62, 88, 92). Activation of the I_h current can underlie this drive toward burst threshold from a hyperpolarized membrane potential. The I_h current typically elicits a depolarizing sag in membrane potential in response to sustained inhibition and can produce a PIR above baseline following removal of the

inhibition (54, 93–96). Here we found that LPG expresses a small amount of PIR in control conditions which is enhanced by Gly¹-SIFamide. This was accompanied by an increased sag potential in Gly¹-SIFamide, suggesting modulation of I_h, which is a target of several neuromodulators in the STNS (46, 97, 98). Furthermore, in the presence of the I_h blocker CsCl, the interburst interval of Gly¹-SIFamide-elicited LPG slow bursts was extended with no consistent effect on burst duration. Similar contributions of I_h to interburst interval occur in the lobster pyloric network (dopamine modulation) and leech heartbeat system (myomodulin peptide modulation) (46, 99). In the LPG neuron, it appears that I_h can speed up the rate of depolarization to the next burst, but it is not necessary for slow intrinsic bursting.

In many bursting neurons, a voltage-dependent, persistent current contributes to maintaining activity during the burst. In particular, a non-inactivating modulator activated, voltage-dependent, mixed cation inward current (I_{MI}) is an important contributor to fast (pyloric) and slow (gastric mill) bursting in STG neurons (72, 100–104). Similarly, in chewing, respiratory, and locomotor network neurons in rodents and leeches, a persistent Na⁺ current supports bursting (89, 105–107). The I_{MI} current is activated by many peptides in the STNS, however there is no effective blocker for this current (73, 103). We did not perform voltage clamp analyses in this study and therefore did not determine if I_{MI}, or the newly identified transient I_{MI} (I_{MI-T}) (73) is a target of Gly¹-SIFamide. However, we tested whether the I_{NaP} blocker riluzole impacted Gly¹-SIFamide-elicited LPG bursting. We found that slow intrinsic LPG bursting was still elicited but the duration of Gly¹-SIFamide-elicited bursts was decreased in riluzole, without an effect on the interburst interval. This suggests that I_{NaP} is important for burst

maintenance but not burst onset. I_{NaP} is present in the LPG neuron in lobster and in unidentified cultured lobster STG neurons (68, 70). Although I_h and I_{NaP} have complementary roles (burst initiation and maintenance, respectively), applying both CsCl and rilzuole was not sufficient to block Gly¹-SIFamide-elicited bursting. This may be due to incomplete block, or Gly¹-SIFamide modulation of an additional current such as I_{MI}.

Gly¹-SIFamide does modulate additional intrinsic properties and thus, likely additional currents. In particular, this peptide decreased the extent of SFA in LPG. SFA can contribute to intraburst firing frequency and burst duration, and often plays an important role in regulating burst termination (59, 60, 108). There was also a general increase in LPG excitability, measured as a larger F/I ratio, which may be due to the same or additional mechanisms as those underlying the decreased SFA. The increased excitability and enhanced firing during Gly¹-SIFamide application may contribute to the ability of LPG to maintain a burst even when its electrically coupled partners AB and PD terminate their pyloric-timed bursts. Calcium activated K⁺ current(s) (IkCa) often contribute to SFA and their modulation can regulate bursting (59, 89, 108–110). SFA was decreased, but not eliminated in Gly¹-SIFamide and thus may be a contributing factor in burst termination. A role for the outward IkCa is supported by the progressive depolarization of the LPG trough that we found during Gly¹-SIFamide application in low Ca²+ saline.

In addition to a progressive depolarization of the LPG trough, LPG slow bursting was greatly reduced in the isolated condition or eliminated entirely in the intact pyloric network condition when Gly¹-SIFamide was applied in low Ca²+ saline. This further

supports a role of I_{KCa}. If there is not sufficient calcium influx to activate I_{KCa}, the membrane potential is not sufficiently hyperpolarized to activate I_h, or to de-inactivate other inward currents and there is no, or weakened, drive to initiate a new burst. However, it is also possible that a calcium current more directly contributes to the LPG slow bursting. One possibility for this is the transient, low-threshold calcium-dependent current (I_{Trans-LTs}). The slow activation of I_{Trans-LTs} can provide a depolarizing influence that, when combined with another inward current such as I_h, is sufficient to initiate bursts in the gastric mill neuron LG in the crab STNS on a similar time scale as LPG slow-bursting (72). Further, the transient nature of I_{Trans-LTs} and its ability to recruit outward currents may contribute to burst termination (72, 73). Involvement of the calcium-dependent I_{Trans-LTs} would be consistent with the decline in burst quality we found in low Ca²⁺ saline. A possible dual contribution of I_h and I_{Trans-LTs} to PIR in LPG may also explain why cesium blockade of I_h extended the interburst interval but did not block intrinsic bursting.

Co-modulation of multiple properties

A balance of inward and outward currents is necessary for intrinsic bursting (102, 111, 112). Thus, it is not surprising that Gly¹-SlFamide would modulate more than one intrinsic property and thus more than one intrinsic current. Correlations occur between ion channels at the mRNA and conductance levels in multiple cell types (81, 113–115). Co-modulation of multiple intrinsic properties, which can maintain such correlations, appears to be important for increasing the range over which rhythmic networks produce stable oscillations (111). For the LPG neuron, and other dual-frequency oscillators, it is

not only a balance of multiple intrinsic currents, but also a balance between intrinsic and synaptic currents that is likely necessary to enable oscillations at both frequencies.

In the intact dual-network condition, LPG receives fast rhythmic electrical coupling input from the AB/PD neurons (38, 48). We found differential importance of I_{NaP} and calcium-related currents in the isolated LPG versus intact network conditions. The inability of LPG to periodically escape the rhythmic electrical input in the presence of riluzole suggests that the electrical synaptic input can dominate LPG activity without an additional inward current such as a persistent sodium current. This could either be due directly to the inward current, or due to the additional leak decreasing the efficacy of the electrical coupling current during LPG slow bursts.

It is not yet known if Gly¹-SIFamide modulates gap junctions. This is a possibility as electrical synapses can be modulated by both amines and peptides (116, 117). In snail neurons, simulated addition of electrical synapses through dynamic clamp supported bistability and dual network activity (118). Additionally, changes in ionic currents and input resistance can alter coupling between cells (119–121). This may explain why LPG could not periodically escape the pyloric rhythm when I_{NaP} was blocked. If this is the case, it is possible that Gly¹-SIFamide may regulate electrical synapses through multiple pathways – both directly and indirectly through modulation of other currents. Regardless of the mechanism, changes in functional coupling strength may be necessary for enabling slow bursts.

Functional Implications

In the STNS, distinct gastric mill rhythms are triggered by different sensory pathways via activation of modulatory projections neurons (122–125). MCN5 is activated by some of these pathways including mechanoreceptors that signal distention of the foregut due to food ingestion, chemosensory neurons, and a proprioceptive muscle tendon organ in the crabs *C. borealis* and *Cancer pagurus* (123, 125). The function of the MCN5/Gly¹-SIFamide gastric mill rhythm is not known. However, MCN5 is strongly activated during sensory neuron activity while other projection neurons are modulated to generate strong, persisting activity following sensory neuron activation (58, 125, 126). Thus, the recruitment of the typically pyloric-only LPG neuron into the gastric mill rhythm may be important for the initial stages of chewing food when the bolus is particularly large.

Network switching extends the functional range of networks and enables changes in the coordination between networks (4, 8, 11, 14, 87). Neuromodulation is suggested to elicit rapid rhythmic network reconfiguration among larger circuits as well. For example, norepinephrine appears to contribute to rapid changes in synchronization of multiple vertebrate brain regions during switches in attention (14, 86, 127). Disordered inter-network coordination and decreased flexibility in oscillatory networks can lead to dysphagia, memory and locomotor deficits, and disruption of cognitive processes (2, 5, 128). Our findings highlight the importance of considering modulation of intrinsic properties (8, 29), either alone, or in combination with modulation of synaptic properties, when investigating mechanisms underlying flexibility of network participation among related networks in other systems.

ENDNOTE

750

At the request of the author(s), readers are herein alerted to the fact that additional
materials related to this manuscript may be found at
https://github.com/blitzdm/Snyder_Blitz_2022. These materials are not a part of this
manuscript and have not undergone peer review by the American Physiological Society
(APS). APS and the journal editors take no responsibility for these materials, for the
website address, or for any links to or from it.

- 757 References
- Stickford ASL, Stickford JL. Ventilation and Locomotion in Humans:
 Mechanisms, Implications, and Perturbations to the Coupling of These Two
 Rhythms. Springer Sci Rev 2014 21 2: 95–118, 2014. doi: 10.1007/S40362-014-0020-4.
- Rangel LM, Rueckemann JW, Riviere PD, Keefe KR, Porter BS, Heimbuch IS,
 Budlong CH, Eichenbaum H. Rhythmic coordination of hippocampal neurons
 during associative memory processing. *Elife* 5: 1–24, 2016. doi:
 10.7554/eLife.09849.
- Roopun AK, Kramer MA, Carracedo LM, Kaiser M, Davies CH, Traub RD,
 Kopell NJ, Whittington MA. Temporal Interactions between Cortical Rhythms.
 Front Neurosci 2: 145–154, 2008. doi: 10.3389/neuro.01.034.2008.
- Dickinson PS. Interactions among neural networks for behavior. *Curr Opin Neurobiol* 5: 792–798, 1995. doi: 10.1016/0959-4388(95)80108-1.
- 5. **Barlow SM**. Central pattern generation involved in oral and respiratory control for feeding in the term infant. *Curr Opin Otolaryngol Head Neck Surg* 17: 187–193, 2009. doi: 10.1097/MOO.0B013E32832B312A.
- Cropper EC, Jing J, Perkins MH, Weiss KR. Use of the aplysia feeding network to study repetition priming of an episodic behavior. *J Neurophysiol* 118: 1861–1870, 2017.
- 77. **Fahoum SRH**, **Blitz DM**. Neuronal switching between single- And dual-network activity via modulation of intrinsic membrane properties. *J Neurosci* 41: 7848–779 7863, 2021. doi: 10.1523/JNEUROSCI.0286-21.2021.
- 780 8. **Tryba AK**, **Peña F**, **Lieske SP**, **Viemari JC**, **Thoby-Brisson M**, **Ramirez JM**.
 781 Differential modulation of neural network and pacemaker activity underlying
 782 eupnea and sigh-breathing activities. *J Neurophysiol* 99: 2114–2125, 2008. doi: 10.1152/jn.01192.2007.
- Weimann JM, Meyrand P, Marder E. Neurons that form multiple pattern
 generators: identification and multiple activity patterns of gastric/pyloric neurons in
 the crab stomatogastric system. *J Neurophysiol* 65: 111–122, 1991. doi:
 10.1152/JN.1991.65.1.111.
- 788 10. **Steriade M, Nunez A, Amzica F**. Intracellular analysis of relations between the slow (. *J Neurosci* 13: 3266–3283, 1993. doi: 10.1523/JNEUROSCI.13-08-03266.1993.
- 791 11. **Meyrand P, Simmers J**, **Moulins M**. Dynamic construction of a neural network from multiple pattern generators in the lobster stomatogastric nervous system. *J Neurosci* 14: 630–644, 1994. doi: 10.1523/jneurosci.14-02-00630.1994.
- 12. **Hooper SL**, **Moulins M**. Cellular and synaptic mechanisms responsible for a long-lasting restructuring of the lobster pyloric network. *J Neurophysiol* 64: 1574–

- 796 1589, 1990. doi: 10.1152/JN.1990.64.5.1574.
- 797 13. **Briggman KL**, **Kristan WB**. Multifunctional pattern-generating circuits. *Annu Rev Neurosci* 31: 271–294, 2008. doi: 10.1146/annurev.neuro.31.060407.125552.
- Bouret S, Sara SJ. Network reset: a simplified overarching theory of locus coeruleus noradrenaline function. *Trends Neurosci* 28: 574–582, 2005. doi: 10.1016/J.TINS.2005.09.002.
- Oku Y, Tanaka I, Ezure K. Activity of bulbar respiratory neurons during fictive coughing and swallowing in the decerebrate cat. *J Physiol* 480: 309–324, 1994. doi: 10.1113/JPHYSIOL.1994.SP020361.
- Shannon R, Baekey DM, Morris KF, Lindsey BG. Ventrolateral medullary respiratory network and a model of cough motor pattern generation. *J Appl Physiol* 84: 2020–2035, 1998. doi: 10.1152/jappl.1998.84.6.2020.
- Lieske SP, Thoby-Brisson M, Telgkamp P, Ramirez JM. Reconfiguration of the neural network controlling multiple breathing patterns: eupnea, sighs and gasps. *Nat Neurosci 2000 36* 3: 600–607, 2000. doi: 10.1038/75776.
- 18. **Lancaster WC**, **Henson OW**, **Keating AW**. Respiratory muscle activity in relation to vocalization in flying bats. *J Exp Biol* 198: 175–191, 1995. doi: 10.1242/JEB.198.1.175.
- Wei XP, Collie M, Dempsey B, Fortin G, Yackle K. A novel reticular node in the brainstem synchronizes neonatal mouse crying with breathing. *Neuron* 110: 644-657.e6, 2022. doi: 10.1016/j.neuron.2021.12.014.
- Yagi N, Oku Y, Nagami S, Yamagata Y, Kayashita J, Ishikawa A, Domen K, Takahashi R. Inappropriate Timing of Swallow in the Respiratory Cycle Causes Breathing-Swallowing Discoordination. *Front Physiol* 8, 2017. doi: 10.3389/FPHYS.2017.00676.
- Stein W, Harzsch S. The Neurobiology of Ocean Change insights from decapod crustaceans. *Zoology* 144, 2021. doi: 10.1016/j.zool.2020.125887.
- Clemens S, Combes D, Meyrand P, Simmers J. Long-term expression of two interacting motor pattern-generating networks in the stomatogastric system of freely behaving lobster. *J Neurophysiol* 79: 1396–1408, 1998. doi: 10.1152/JN.1998.79.3.1396.
- Saunders SW, Rath D, Hodges PW. Postural and respiratory activation of the trunk muscles changes with mode and speed of locomotion. *Gait Posture* 20: 280–290, 2004. doi: 10.1016/j.gaitpost.2003.10.003.
- Gutierrez GJ, O'Leary T, Marder E. Multiple mechanisms switch an electrically coupled, synaptically inhibited neuron between competing rhythmic oscillators.

 Neuron 77: 845–858, 2013. doi: 10.1016/J.NEURON.2013.01.016.
- Nadim F, Bucher D. Neuromodulation of neurons and synapses. *Curr Opin Neurobiol* 29: 48–56, 2014. doi: 10.1016/j.conb.2014.05.003.

- Harris-Warrick RM. Neuromodulation and flexibility in Central Pattern Generator networks. *Curr. Opin. Neurobiol.* 21 Elsevier Current Trends: 685–692, 2011.
- 837 27. **Marder E, Thirumalai V**. Cellular, synaptic and network effects of neuromodulation. *Neural Netw* 15: 479–493, 2002. doi: 10.1016/S0893-6080(02)00043-6.
- Faumont S, Combes D, Meyrand P, Simmers J. Reconfiguration of multiple motor networks by short- and long-term actions of an identified modulatory neuron. *Eur J Neurosci* 22: 2489–2502, 2005. doi: 10.1111/J.1460-9568.2005.04442.X.
- Drion G, Franci A, Sepulchre R. Cellular switches orchestrate rhythmic circuits.
 Biol Cybern 113: 71–82, 2019. doi: 10.1007/S00422-018-0778-6.
- 30. **Daur N**, **Nadim F**, **Bucher D**. The complexity of small circuits: the stomatogastric nervous system. *Curr Opin Neurobiol* 41: 1–7, 2016. doi: 10.1016/J.CONB.2016.07.005.
- 849 31. **Marder E**, **Bucher D**. Understanding circuit dynamics using the stomatogastric nervous system of lobsters and crabs. *Ann Rev Physiol* 69: 2007.
- Stein W. Modulation of stomatogastric rhythms. *J Comp Physiol A Neuroethol Sens Neural Behav Physiol* 195: 989–1009, 2009. doi: 10.1007/S00359-009-0483-Y.
- 854 33. **Nusbaum MP**. Modulatory Projection Neurons. .
- Stehlik LL. Diets of the brachyuran crabs *Cancer irroratus, C. borealis*, and
 Ovalipes ocellatus in the New York Bight. *J Crustac Biol* 13: 723–735, 1993. doi: 10.1163/193724093x00291.
- B58 35. **Dickinson PS**, **Stemmler EA**, **Christie AE**. The pyloric neural circuit of the herbivorous crab *Pugettia producta* shows limited sensitivity to several neuromodulators that elicit robust effects in more opportunistically feeding decapods. *J Exp Biol* 211: 1434–1447, 2008. doi: 10.1242/JEB.016998.
- B62 36. Donahue MJ, Nichols A, Santamaria CA, League-Pike PE, Krediet CJ, Perez KO, Shulman MJ. Predation Risk, Prey Abundance, and the Vertical Distribution of Three Brachyuran Crabs on Gulf of Maine Shores. *J Crustac Biol* 29: 523–531, 2009. doi: 10.1651/08-3061.1.
- Blitz DM, Christie AE, Cook AP, Dickinson PS, Nusbaum MP. Similarities and differences in circuit responses to applied Gly¹-SIFamide and peptidergic (Gly¹ SIFamide) neuron stimulation. *J Neurophysiol* 121: 950–972, 2019. doi: 10.1152/jn.00567.2018.
- 870 38. **Shruti S, Schulz DJ**, **Lett KM**, **Marder E**. Electrical coupling and innexin expression in the stomatogastric ganglion of the crab Cancer borealis. *J Neurophysiol* 112: 2946–2958, 2014. doi: 10.1152/JN.00536.2014.
- 873 39. **Gutierrez GJ**, **Grashow RG**. Cancer borealis stomatogastric nervous system

- dissection. *J Vis Exp* , 2009. doi: 10.3791/1207.
- Hamood AW, Haddad SA, Otopalik AG, Rosenbaum P, Marder E. Quantitative reevaluation of the effects of short- and long-term removal of descending modulatory inputs on the pyloric rhythm of the crab, *Cancer borealis*. *eNeuro* 2, 2015. doi: 10.1523/ENEURO.0058-14.2015.
- Hamood AW, Marder E. Consequences of acute and long-term removal of
 neuromodulatory input on the episodic gastric rhythm of the crab Cancer borealis.
 J Neurophysiol 114: 1677–1692, 2015. doi: 10.1152/JN.00536.2015.
- Tohidi V, Nadim F. Membrane resonance in bursting pacemaker neurons of an oscillatory network is correlated with network frequency. *J Neurosci* 29: 6427–6435, 2009. doi: 10.1523/JNEUROSCI.0545-09.2009.
- 885 43. **Pérez-Acevedo NL**, **Krenz WD**. Metabotropic glutamate receptor agonists modify 886 the pyloric output of the crustacean stomatogastric ganglion. 1062: 1–8, 2005. 887 doi: 10.1016/J.BRAINRES.2005.06.061.
- Stein W, Eberle CC, Hedrich UBS. Motor pattern selection by nitric oxide in the stomatogastric nervous system of the crab. *Eur J Neurosci* 21: 2767–2781, 2005. doi: 10.1111/j.1460-9568.2005.04117.x.
- Scholz NL, De Vente J, Truman JW, Graubard K. Neural Network Partitioning
 by NO and cGMP. *J Neurosci* 21: 1610, 2001. doi: 10.1523/JNEUROSCI.21-05-01610.2001.
- Peck JH, Gaier E, Stevens E, Repicky S, Harris-Warrick RM. Amine
 modulation of Ih in a small neural network. *J Neurophysiol* 96: 2931–2940, 2006.
 doi: 10.1152/JN.00423.2005.
- Zhu L, Selverston AI, Ayers J. Role of Ih in differentiating the dynamics of the
 gastric and pyloric neurons in the stomatogastric ganglion of the lobster, *Homarus* americanus. J Neurophysiol 115: 2434–2445, 2016. doi: 10.1152/JN.00737.2015.
- 900 48. **Marder E, Eisen JS**. Transmitter identification of pyloric neurons: electrically coupled neurons use different transmitters. *J Neurophysiol* 51: 1345–1361, 1984. doi: 10.1152/JN.1984.51.6.1345.
- 49. Hooper SL, Thuma JB, Guschlbauer C, Schmidt J, Büschges A. Cell dialysis
 by sharp electrodes can cause nonphysiological changes in neuron properties. J
 Neurophysiol 114: 1255–1271, 2015. doi: 10.1152/JN.01010.2014.
- Hudson AE, Archila S, Prinz AA. Identifiable cells in the crustacean
 stomatogastric ganglion. *Physiology* 25: 311–318, 2010. doi:
 10.1152/PHYSIOL.00019.2010/ASSET/IMAGES/LARGE/PHY0041000230003.JP
 EG.
- 910 51. Opdyke CA, Calabrese RL. Outward currents in heart motor neurons of the
 911 medicinal leech. *J Neurophysiol* 74: 2524–2537, 1995. doi:
 912 10.1152/jn.1995.74.6.2524.

- 913 52. **Marder E, Gutierrez GJ, Nusbaum MP**. Complicating connectomes: Electrical coupling creates parallel pathways and degenerate circuit mechanisms. *Dev Neurobiol* 77: 597–609, 2017.
- 916 53. **Blitz DM**. Circuit feedback increases activity level of a circuit input through interactions with intrinsic properties. *J Neurophysiol* 118: 949–963, 2017. doi: 10.1152/jn.00772.2016.
- 919 54. **Angstadt JD**, **Grassmann JL**, **Theriault KM**, **Levasseur SM**. Mechanisms of postinhibitory rebound and its modulation by serotonin in excitatory swim motor neurons of the medicinal leech. *J Comp Physiol A Neuroethol Sens Neural Behav Physiol* 191: 715–732, 2005. doi: 10.1007/S00359-005-0628-6.
- 923 55. Bidaut M. Pharmacological dissection of pyloric network of the lobster
 924 stomatogastric ganglion using picrotoxin. *J Neurophysiol* 44: 1089–1101, 1980.
 925 doi: 10.1152/JN.1980.44.6.1089.
- 926 56. **Cleland TA**, **Selverston AI**. Glutamate-gated inhibitory currents of central pattern 927 generator neurons in the lobster stomatogastric ganglion. *J Neurosci* 15: 6631– 928 6639, 1995. doi: 10.1523/JNEUROSCI.15-10-06631.1995.
- 929 57. **Bartos M**, **Manor Y**, **Nadim F**, **Marder E**, **Nusbaum MP**. Coordination of fast and slow rhythmic neuronal circuits. *J Neurosci* 19: 6650–6660, 1999.
- 931 58. **Blitz DM**, **White RS**, **Saideman SR**, **Cook A**, **Christie AE**, **Nadim F**, **Nusbaum**932 **MP**. A newly identified extrinsic input triggers a distinct gastric mill rhythm via
 933 activation of modulatory projection neurons. *J Exp Biol* 211: 1000–1011, 2008.
 934 doi: 10.1242/jeb.015222.
- 935 59. **Ha GE**, **Cheong E**. Spike Frequency Adaptation in Neurons of the Central Nervous System. *Exp Neurobiol* 26: 179–185, 2017.
- 60. **Katz PS**, **Frost WN**. Removal of spike frequency adaptation via neuromodulation intrinsic to the *Tritonia* escape swim central pattern generator. *J Neurosci* 17: 7703–7713, 1997. doi: 10.1523/JNEUROSCI.17-20-07703.1997.
- 940 61. **Madison D V.**, **Nicoll RA**. Noradrenaline blocks accommodation of pyramidal cell discharge in the hippocampus. *Nature* 299: 636–638, 1982. doi: 10.1038/299636A0.
- 943 62. **Bucher D**, **Haspel G**, **Golowasch J**, **Nadim F**. Central pattern generators. .
- Tong H, McDearmid JR. Pacemaker and plateau potentials shape output of a developing locomotor network. *Curr Biol* 22: 2285–2293, 2012. doi: 10.1016/J.CUB.2012.10.025.
- 947 64. **Picton LD**, **Sillar KT**, **Zhang HY**. Control of *Xenopus* Tadpole Locomotion via 948 Selective Expression of Ih in Excitatory Interneurons. *Curr Biol* 28: 3911-3923.e2, 949 2018. doi: 10.1016/J.CUB.2018.10.048.
- 65. **Combe CL**, **Gasparini S**. I h from synapses to networks: HCN channel functions and modulation in neurons. *Prog Biophys Mol Biol* 166: 119–132, 2021. doi:

- 952 10.1016/J.PBIOMOLBIO.2021.06.002.
- Harris-Warrick RM. Voltage-sensitive ion channels in rhythmic motor systems.
 Curr Opin Neurobiol 12: 646–651, 2002. doi: 10.1016/S0959-4388(02)00377-X.
- Zhang Y, Oliva R, Gisselmann G, Hatt H, Guckenheimer J, Harris-Warrick
 RM. Overexpression of a hyperpolarization-activated cation current (lh) channel
 gene modifies the firing activity of identified motor neurons in a small neural
 network. *J Neurosci* 23: 9059–9067, 2003. doi: 10.1523/JNEUROSCI.23-27-09059.2003.
- 960 68. **Elson RC**, **Selverston AI**. Evidence for a persistent Na+ conductance in neurons of the gastric mill rhythm generator of spiny lobsters. *J Exp Biol* 200: 1795–1807, 1997. doi: 10.1242/JEB.200.12.1795.
- Angstadt JD, Simone AM. Riluzole suppresses postinhibitory rebound in an
 excitatory motor neuron of the medicinal leech. *J Comp Physiol A Neuroethol* Sens Neural Behav Physiol 200: 759–775, 2014. doi: 10.1007/S00359-014-0919 X.
- 70. **Turrigiano G**, **LeMasson G**, **Marder E**. Selective regulation of current densities underlies spontaneous changes in the activity of cultured neurons. *J Neurosci* 15: 3640–3652, 1995. doi: 10.1523/JNEUROSCI.15-05-03640.1995.
- 970 71. **Schuster JE**, **Fu R**, **Siddique T**, **Heckman CJ**. Effect of prolonged riluzole 971 exposure on cultured motoneurons in a mouse model of ALS. *J Neurophysiol* 107: 972 484, 2012. doi: 10.1152/JN.00714.2011.
- 973 72. **Rodriguez JC**, **Blitz DM**, **Nusbaum MP**. Convergent rhythm generation from divergent cellular mechanisms. *J Neurosci* 33: 18047–18064, 2013. doi: 10.1523/JNEUROSCI.3217-13.2013.
- 976 73. **Schneider AC**, **Fox D**, **Itani O**, **Golowasch J**, **Bucher D**, **Nadim F**. Frequency-977 Dependent Action of Neuromodulation. *eNeuro* 8, 2021. doi: 978 10.1523/ENEURO.0338-21.2021.
- 979 74. **Russell DF**, **Hartline DK**. Slow active potentials and bursting motor patterns in pyloric network of the lobster, *Panulirus interruptus*. *J Neurophysiol* 48: 914–937, 1982. doi: 10.1152/JN.1982.48.4.914.
- Je T, Verley DR, Goaillard JM, Messinger DI, Christie AE, Birmingham JT.
 Bistable behavior originating in the axon of a crustacean motor neuron. *J Neurophysiol* 95: 1356–1368, 2006. doi: 10.1152/JN.00893.2005.
- 985 76. **Guinamard R, Simard C, Del Negro C**. Flufenamic acid as an ion channel modulator. *Pharmacol Ther* 138: 272–284, 2013. doi: 10.1016/J.PHARMTHERA.2013.01.012.
- Coleman MJ, Meyrand P, Nusbaum MP. A switch between two modes of
 synaptic transmission mediated by presynaptic inhibition. *Nature* 378: 502–505,
 1995. doi: 10.1038/378502a0.

- 991 78. **Blitz DM**, **Nusbaum MP**. Distinct functions for cotransmitters mediating motor pattern selection. *J Neurosci* 19: 6774–6783, 1999. doi: 10.1523/jneurosci.19-16-06774.1999.
- 994 79. **Beenhakker MP**, **Kirby MS**, **Nusbaum MP**. Mechanosensory gating of proprioceptor input to modulatory projection neurons. *J Neurosci* 27: 14308–996 14316, 2007. doi: 10.1523/JNEUROSCI.4404-07.2007.
- Hooper SL, O'Neil MB, Wagner R, Ewer J, Golowasch J, Marder E. The innervation of the pyloric region of the crab, *Cancer borealis*: homologous muscles in decapod species are differently innervated. *J Comp Physiol A* 159: 227–240, 1986. doi: 10.1007/BF00612305.
- 1001 81. **Khorkova O, Golowasch J**. Neuromodulators, not activity, control coordinated expression of ionic currents. *J Neurosci* 27: 8709–8718, 2007. doi: 10.1523/JNEUROSCI.1274-07.2007.
- Golowasch J, Marder E. lonic currents of the lateral pyloric neuron of the stomatogastric ganglion of the crab. *J Neurophysiol* 67: 318–331, 1992. doi: 10.1152/JN.1992.67.2.318.
- Nagy F, Dickinson PS. Control of a central pattern generator by an identified modulatory interneurone in crustacea. I. Modulation of the pyloric motor output. *J Exp Biol* 105: 33–58, 1983. doi: 10.1242/JEB.105.1.33.
- Dickinson PS, Mecsas C, Marder E. Neuropeptide fusion of two motor-pattern generator circuits. *Nature* 344: 155–158, 1990. doi: 10.1038/344155A0.
- Bartlett D, Leiter JC. Coordination of Breathing with Nonrespiratory Activities. Compr Physiol 2: 1387–1415, 2012. doi: 10.1002/CPHY.C110004.
- Oyarzabal EA, Hsu LM, Das M, Chao THH, Zhou J, Song S, Zhang W, Smith KG, Sciolino NR, Evsyukova IY, Yuan H, Lee SH, Cui G, Jensen P, Shih YYI.
 Chemogenetic stimulation of tonic locus coeruleus activity strengthens the default mode network. *Sci Adv* 8, 2022. doi: 10.1126/SCIADV.ABM9898.
- 1018 87. **Weimann JM**, **Marder E**. Switching neurons are integral members of multiple oscillatory networks. *Curr Biol* 4: 896–902, 1994. doi: 10.1016/S0960-1020 9822(00)00199-8.
- Marder E, Calabrese RL. Principles of rhythmic motor pattern generation. *Physiol Rev* 76: 687–717, 1996. doi: 10.1152/PHYSREV.1996.76.3.687.
- Harris-Warrick RM. General principles of rhythmogenesis in central pattern generator networks. In: *Progress in Brain Research*. Elsevier, 2010, p. 213–222.
- 90. **Peña F, Parkis MA**, **Tryba AK**, **Ramirez JM**. Differential contribution of pacemaker properties to the generation of respiratory rhythms during normoxia and hypoxia. *Neuron* 43: 105–117, 2004. doi: 10.1016/j.neuron.2004.06.023.
- 1028 91. **Adams WB**, **Benson JA**. The generation and modulation of endogenous rhythmicity in the Aplysia bursting pacemaker neurone R15. *Prog Biophys Mol*

- 1030 *Biol* 46: 1–49, 1985. doi: 10.1016/0079-6107(85)90011-2.
- 1031 92. Lu AC, Lee CK, Kleiman-Weiner M, Truong B, Wang M, Huguenard JR,
 1032 Beenhakker MP. Nonlinearities between inhibition and T-type calcium channel activity bidirectionally regulate thalamic oscillations. *Elife* 9: 1–36, 2020. doi: 10.7554/ELIFE.59548.
- Hogan QH, Poroli M. Hyperpolarization-activated current (I(h)) contributes to excitability of primary sensory neurons in rats. *Brain Res* 1207: 102–110, 2008. doi: 10.1016/J.BRAINRES.2008.02.066.
- Goaillard JM, Taylor AL, Pulver SR, Marder E. Slow and persistent postinhibitory rebound acts as an intrinsic short-term memory mechanism. *J Neurosci* 30: 4687–4692, 2010. doi: 10.1523/JNEUROSCI.2998-09.2010.
- Yang SS, Li YC, Coley AA, Chamberlin LA, Yu P, Gao WJ. Cell-Type Specific
 Development of the Hyperpolarization-Activated Current, Ih, in Prefrontal Cortical
 Neurons. Front Synaptic Neurosci 10, 2018. doi: 10.3389/FNSYN.2018.00007.
- Sangrey T, Jaeger D. Analysis of distinct short and prolonged components in rebound spiking of deep cerebellar nucleus neurons. *Eur J Neurosci* 32: 1646–1046 1657, 2010. doi: 10.1111/J.1460-9568.2010.07408.X.
- 97. Ballo AW, Keene JC, Troy PJ, Goeritz ML, Nadim F, Bucher D. Dopamine modulates Ih in a motor axon. *J Neurosci* 30: 8425–8434, 2010. doi: 10.1523/JNEUROSCI.0405-10.2010.
- 1050 98. **Krenz WD**, **Parker AR**, **Rodgers E**, **Baro DJ**. Monoaminergic tone supports conductance correlations and stabilizes activity features in pattern generating neurons of the lobster, *Panulirus interruptus*. *Front Neural Circuits* 9, 2015. doi: 10.3389/fncir.2015.00063.
- 1054 99. **Tobin AE**, **Calabrese RL**. Myomodulin increases Ih and inhibits the NA/K pump to modulate bursting in leech heart interneurons. *J Neurophysiol* 94: 3938–3950, 2005. doi: 10.1152/JN.00340.2005.
- 100. DeLong ND, Kirby MS, Blitz DM, Nusbaum MP. Parallel regulation of a
 modulator-activated current via distinct dynamics underlies comodulation of motor
 circuit output. *J Neurosci* 29: 12355–12367, 2009. doi:
 10.1523/JNEUROSCI.3079-09.2009.
- 101. **Swensen AM**, **Marder E**. Multiple peptides converge to activate the same voltage-dependent current in a central pattern-generating circuit. *J Neurosci* 20: 6752–6759, 2000. doi: 10.1523/jneurosci.20-18-06752.2000.
- 102. **Golowasch J, Bose A, Guan Y, Salloum D, Roeser A, Nadim F**. A balance of outward and linear inward ionic currents is required for generation of slow-wave oscillations. *J Neurophysiol* 118: 1092–1104, 2017. doi: 10.1152/JN.00240.2017.
- 103. **Gray M**, **Daudelin DH**, **Golowasch J**. Activation mechanism of a neuromodulator-gated pacemaker ionic current. *J Neurophysiol* 118: 595–609, 2017. doi: 10.1152/JN.00743.2016.

- 104. **Kintos N**, **Nusbaum MP**, **Nadim F**. Convergent neuromodulation onto a network neuron can have divergent effects at the network level. *J Comput Neurosci* 40: 113–135, 2016. doi: 10.1007/S10827-015-0587-Z.
- 1073 105. **Crisp KM**, **Gallagher BR**, **Mesce KA**. Mechanisms contributing to the dopamine induction of crawl-like bursting in leech motoneurons. *J Exp Biol* 215: 3028–3036, 2012. doi: 10.1242/JEB.069245.
- 106. **Tazerart S, Vinay L, Brocard F**. The persistent sodium current generates pacemaker activities in the central pattern generator for locomotion and regulates the locomotor rhythm. *J Neurosci* 28: 8577–8589, 2008. doi: 10.1523/JNEUROSCI.1437-08.2008.
- 107. **Yamanishi T, Koizumi H, Navarro MA, Milescu LS, Smith JC**. Kinetic properties of persistent Na + current orchestrate oscillatory bursting in respiratory neurons. *J Gen Physiol* 150: 1523–1540, 2018. doi: 10.1085/JGP.201812100.
- 108. **El Manira A**, **Tegner J**, **Grillner S**. Calcium-dependent potassium channels play a critical role for burst termination in the locomotor network in lamprey. *J Neurophysiol* 72: 1852–1861, 1994. doi: 10.1152/jn.1994.72.4.1852.
- 1086 109. **Ramirez JM**, **Doi A**, **Garcia AJ**, **Elsen FP**, **Koch H**, **Wei AD**. The cellular building blocks of breathing. *Compr Physiol* 2: 2683–2731, 2012. doi: 10.1002/CPHY.C110033.
- 1089 110. **Overton PG**, **Clark D**. Burst firing in midbrain dopaminergic neurons. *Brain Res* Rev 25: 312–334, 1997. doi: 10.1016/S0165-0173(97)00039-8.
- 1091 111. **Ellingson PJ**, **Barnett WH**, **Kueh D**, **Vargas A**, **Calabrese RL**, **Cymbalyuk GS**.
 1092 Comodulation of h- and Na +/K + Pump Currents Expands the Range of
 1093 Functional Bursting in a Central Pattern Generator by Navigating between
 1094 Dysfunctional Regimes. *J Neurosci* 41: 6468–6483, 2021. doi:
 10.1523/JNEUROSCI.0158-21.2021.
- 1096 112. **Amarillo Y, Zagha E, Mato G, Rudy B, Nadal MS**. The interplay of seven subthreshold conductances controls the resting membrane potential and the oscillatory behavior of thalamocortical neurons. *J Neurophysiol* 112: 393–410, 2014. doi:
- 10.1152/JN.00647.2013/ASSET/IMAGES/LARGE/Z9K0141424940011.JPEG.
- 1101 113. **Yang J**, **Shakil H**, **Ratté S**, **Prescott SA**. Minimal requirements for a neuron to coregulate many properties and the implications for ion channel correlations and robustness. *Elife* 11, 2022. doi: 10.7554/ELIFE.72875.
- 1104 114. **Schulz DJ**, **Goaillard JM**, **Marder E**. Variable channel expression in identified single and electrically coupled neurons in different animals. *Nat Neurosci* 9: 356–362, 2006. doi: 10.1038/NN1639.
- 115. **Tran T, Unal CT, Severin D, Zaborszky L, Rotstein HG, Kirkwood A,**1108 **Golowasch J**. Ionic current correlations are ubiquitous across phyla. *Sci Rep* 9,
 1109 2019. doi: 10.1038/S41598-018-38405-6.

- 1110 116. **Lane BJ**, **Kick DR**, **Wilson DK**, **Nair SS**, **Schulz DJ**. Dopamine maintains network synchrony via direct modulation of gap junctions in the crustacean cardiac ganglion. *Elife* 7, 2018. doi: 10.7554/ELIFE.39368.
- 1113 117. **Zsiros V, Maccaferri G**. Noradrenergic modulation of electrical coupling in GABAergic networks of the hippocampus. *J Neurosci* 28: 1804–1815, 2008. doi: 10.1523/JNEUROSCI.4616-07.2008.
- 1116 118. **Bem T, Le Feuvre Y**, **Rinzel J**, **Meyrand P**. Electrical coupling induces bistability of rhythms in networks of inhibitory spiking neurons. *Eur J Neurosci* 22: 2661–1118 2668, 2005. doi: 10.1111/J.1460-9568.2005.04405.X.
- 1119 119. **Nadim F**, **Li X**, **Gray M**, **Golowasch J**. The Role of Electrical Coupling in Rhythm Generation in Small Networks.
- 120. **Alcamí P, Pereda AE**. Beyond plasticity: the dynamic impact of electrical synapses on neural circuits. *Nat Rev Neurosci* 20: 253–271, 2019. doi: 10.1038/S41583-019-0133-5.
- 124 121. **O'Brien J**. The ever-changing electrical synapse. *Curr Opin Neurobiol* 29: 64–72, 2014. doi: 10.1016/J.CONB.2014.05.011.
- 122. **Blitz DM**, **Beenhakker MP**, **Nusbaum MP**. Different sensory systems share projection neurons but elicit distinct motor patterns. *J Neurosci* 24: 11381–11390, 2004. doi: 10.1523/JNEUROSCI.3219-04.2004.
- 123. **Hedrich UBS**, **Smarandache CR**, **Stein W**. Differential activation of projection neurons by two sensory pathways contributes to motor pattern selection. *J Neurophysiol* 102: 2866–2879, 2009. doi: 10.1152/jn.00618.2009.
- 1132 124. **Blitz DM**, **Nusbaum MP**. Modulation of circuit feedback Specifies motor circuit output. *J Neurosci* 32: 9182–9193, 2012. doi: 10.1523/JNEUROSCI.1461-12.2012.
- 125. **Beenhakker MP**, **Blitz DM**, **Nusbaum MP**. Long-Lasting Activation of Rhythmic Neuronal Activity by a Novel Mechanosensory System in the Crustacean Stomatogastric Nervous System. *J Neurophysiol* 91: 78–91, 2004. doi: 10.1152/jn.00741.2003.
- 126. Christie AE, Stein W, Quinlan JE, Beenhakker MP, Marder E, Nusbaum MP.
 Actions of a Histaminergic/Peptidergic Projection Neuron on Rhythmic Motor
 Patterns in the Stomatogastric Nervous System of the Crab Cancer borealis. *J*Comp Neurol 469: 153–169, 2004. doi: 10.1002/cne.11003.
- 127. **Ramirez JM**, **Dashevskiy T**, **Marlin IA**, **Baertsch N**. Microcircuits in respiratory rhythm generation: commonalities with other rhythm generating networks and evolutionary perspectives. *Curr Opin Neurobiol* 41: 53–61, 2016. doi: 10.1016/j.conb.2016.08.003.
- 128. **Moore JD**, **Kleinfeld D**, **Wang F**. How the brainstem controls orofacial behaviors comprised of rhythmic actions. *Trends Neurosci* 37: 370–380, 2014. doi: 10.1016/j.tins.2014.05.001.

129. **Bucher D**, **Goaillard JM**. Beyond faithful conduction: short-term dynamics, neuromodulation, and long-term regulation of spike propagation in the axon. *Prog Neurobiol* 94: 307–346, 2011. doi: 10.1016/J.PNEUROBIO.2011.06.001.

Acknowledgements

We thank Savanna-Rae Fahoum and Barathan Gnanabharathi for reading earlier versions and providing helpful discussions, Michael Hughes and the Statistical Consulting Center at Miami University for assistance with statistical analysis, and Kathleen Killian and Paul James for helpful comments. This work funded by National Science Foundation (IOS: 1755283; DMB) and the Department of Biology at Miami University.

Figure Legends

Figure 1: Modulatory neuron MCN5 or bath application of its neuropeptide Gly¹-SIFamide elicits a switch in LPG neuron activity from only pyloric-timed oscillations to dual pyloric/gastric mill-timed oscillations. A) The isolated stomatogastric nervous system consists of the paired CoGs and single OG from which modulatory neurons originate, and the single STG containing pyloric and gastric mill network neurons. This study used intracellular recordings from network neurons in the STG and extracellular recordings from peripheral nerves (circles on nerves). There is a single MCN5 soma in each CoG which project an axon through the *ion* and *stn* and terminate in the STG. Double lines through *ions* and *sons* indicate cuts made to eliminate modulatory input to the STG from MCN5 and other modulatory neurons located in the CoGs. B) The rhythmogenic pyloric pacemaker ensemble located within the STG consists of a single AB neuron, two PD neurons and two LPG neurons coupled through electrical synapses (resistors, electrical synapses; diode, rectifying electrical synapse). Red circles indicate neurons solely active in the pyloric rhythm, red/blue

circles indicate that LPG can participate in both the pyloric and gastric mill networks. C) Baseline conditions for this study included the presence of the inhibitory glutamate channel antagonist picrotoxin (PTX, 10 µM) to block chemical synaptic input to LPG. In this condition, AB (not shown), PD (bottom, extracellular pdn recording), and LPG (top, intracellular recording) generate rhythmic pyloric-timed (~1 Hz) oscillations (red boxes) due to the intrinsic properties of the AB neuron and the electrical coupling among this pacemaker ensemble (38, 48). In this condition, the gastric-mill rhythm is inactive (not shown). D) In 5 µM Gly¹-SIFamide in PTX, LPG exhibits dual frequency bursting in time with the fast pyloric (~1 Hz; red boxes) and slow gastric mill (~0.1 Hz; blue box) rhythms. E) LPG slow bursts (blue box) occur via intrinsic properties and therefore persist in 5 µM Gly¹-SIFamide in PTX with hyperpolarizing current in the PD neurons (PTX:PD_{hype}) to silence the pyloric rhythm (7). Scale bars apply to C-E. All recordings are from the same preparation. Abbreviations: Ganglia: CoG, commissural ganglion; OG, Oesophageal ganglion; STG, Stomatogastric ganglion. Nerves: ion, inferior oesophageal nerve; *lpgn*, lateral posterior gastric nerve; *on*, oesophageal nerve; *pdn*, pyloric dilator nerve; *son*, superior oesophageal nerve; *stn*, stomatogastric nerve. Neurons: AB, anterior burster; LPG, lateral posterior gastric; MCN5, modulatory commissural neuron 5; PD, pyloric dilator.

1195

1196

1197

1198

1199

1177

1178

1179

1180

1181

1182

1183

1184

1185

1186

1187

1188

1189

1190

1191

1192

1193

Figure 2: LPG excitability was increased by Gly¹-SlFamide. A) LPG input resistance was measured with a 1 nA hyperpolarizing current injection starting near LPG resting potential in the baseline PTX:PDhype condition and matched to the same initial membrane potential in the SIF:PTX:PDhype condition. In an example experiment, LPG

was hyperpolarized more in Gly¹-SIFamide (5 μM; SIF:PTX:PDhype; black trace) compared to PTX:PDhype (grey trace). Each trace is the average of three trials. B) Plot of input resistance in PTX:PDhype (open circles) and SIF:PTX:PDhype (filled circles). Each line with pair of symbols is a single experiment. Gray bars indicate averages for each condition. (**p < 0.01; n = 11; paired t-test). C-D) LPG was depolarized with a 0.5, 1.5, and 2.5 nA current injection for 5 s in PTX:PDhype (Ci-iii) or SIF:PTX:PDhype (Di-Diii). The pre-current step membrane potential was matched between the two conditions using current injection in DCC mode (see Methods). Scale bars between Cii and Dii apply to all traces in C-D. All traces in C-D are from the same experiment. E) The average (± SEM) LPG firing frequency across each level of current injection is plotted for PTX:PDhype (open circles) and for SIF:PTX:PDhype (filled circles). (0.5 – 3.0 nA; *p<0.05, ***p<0.01; 0.5 nA, n = 7; 1.0 nA, n = 10; 1.5 nA, n = 9; 2.0 nA, n = 10; 2.5 nA, n = 8; 3.0 nA, n = 4; Two-way RM ANOVA, Tukey post-hoc).

Figure 3: LPG spike frequency adaptation was decreased by Gly¹-SIFamide. LPG firing frequency was assessed across a 5 s (1.0 nA) current injection in the PTX:PD_{hype} (A) and SIF:PTX:PD_{hype} (B) conditions. (Ai-ii; Bi-ii) Expanded sections from A, B highlight the firing frequency at the beginning (*i*; 0.5 s) and end (*ii*; 0.5 s) of the current step. Scale bar in A applies to A and B. Scale bar in Aii applies to Ai-Bii. All recordings are from the same preparation. C) Plot of interspike interval versus time for all intervals in the example experiment shown in (A) (open circles; PTX:PD_{hype}) and (B) (filled circles; SIF:PTX:PD_{hype}). Linear fits to the data are indicated by the solid (PTX:PD_{hype}) and grey dashed (SIF:PTX:PD_{hype}) lines. (D) The slope of each line across experiments

was then plotted for PTX:PD_{hype} (open circles) and SIF:PTX:PD_{hype} (filled circles). Each line plus set of symbols plots the ISI slopes for a single experiment. Gray bars indicate averages for each condition. (**p = 0.004; n = 9; Wilcoxon signed-rank test).

1226

1227

1228

1229

1230

1231

1232

1233

1234

1235

1236

1237

1238

1239

1240

1241

1223

1224

1225

Figure 4: LPG post-inhibitory rebound was enhanced by Gly¹-SIFamide. A hyperpolarizing current step was used to bring LPG to the same membrane potential in PTX:PD_{hvpe} (Ai) and SIF:PTX:PD_{hvpe} (Aii) for 5 s. The LPG membrane potential sagged upwards (bracket) toward the end of the current step. After the end of the current step, LPG generated a rebound above baseline (grey dashed line) including firing action potentials. The grey shaded areas indicate the analysis region for (B) (see Methods). Scale bars apply to Ai, Aii. Recordings are from the same preparation. B) Plot of integrated area under the curve for each experiment in the presence (filled circles) and absence (open circles) of Gly¹-SIFamide (***p<0.001; n = 8; paired t-test). C) The cumulative number of spikes per bin is plotted across the 4 s window (grey areas in Ai, Aii) for PTX:PD_{hype} (dark grey) and SIF:PTX:PD_{hype} (lighter grey) (Bin size: 0.1 s). D) Plot of sag amplitude (change in membrane potential, see brackets in Ai, Aii; mV) for each experiment in the presence (filled circles) and absence (open circles) of Gly¹-SIFamide. (**p<0.01; n = 8; paired t-test). Gray bars in B, D indicate averages for each condition.

1242

1243

Figure 5: Blocking In current with CsCl increased the interburst interval in Gly¹-SIFamide-elicited LPG intrinsic bursting. Ai) The LPG neurons (single LPG

intracellular: top trace; paired LPGs, extracellular *lpgn*: middle trace) generated intrinsic bursts with the PD neurons hyperpolarized (extracellular pdn: bottom trace) during Gly¹-SIFamide application (SIF:PTX:PD_{hype}). (Aii) In the same preparation, LPG also generated slow bursting when Gly¹-SIFamide was bath-applied in CsCl to block I_h. Scale bars apply to Ai-Aii. The LPG slow burst cycle period (B), interburst interval (C) and burst duration (D) are plotted for SIF:PTX:PD_{hype} before (SIF Pre) and after (SIF Post) SIF:PTX:PD_{hype} in CsCl (SIF CsCl). Ei) In an example preparation, bath-applied Gly¹-SIFamide in PTX with the pyloric rhythm intact (PTX:PD_{on}) elicited periodic slow bursts that escape the pyloric rhythm and persisted for multiple pyloric cycles (PD neuron bursts, pdn). The membrane potential of pyloric-timed troughs in LPG between slow bursts progressively depolarized preceding a slow burst (dotted line). Eii) In the same preparation, application of Gly¹-SIFamide with CsCl in the PTX:PD_{on} condition also elicited periodic slow bursts that escaped from the pyloric rhythm. In this condition, there was not a progressive depolarization of the trough membrane potential leading to the next slow burst (dotted line). Scale bars apply to Ei-Eii. Cycle period (F), interburst interval (G), and burst duration (H) during SIF:PTX:PDhype before (SIF Pre), during (SIF CsCl), and after (SIF Post) SIF:PTX:PDon in CsCl. Black bars above traces highlight the first interburst interval duration in SIF:PTX:PD_{hype/on} for comparison with the CsCl condition in A and E. In all graphs, each set of circles and lines connect data points from a single experiment and gray bars represent mean values for each condition. (SIF:PTX:PDon, black circles; CsCl + SIF:PTX:PDon, green circles). (B-D, n = 8; F-H, n = 7-8; *p<0.05, **p<0.01. ***p<0.001; one-way RM ANOVA, Holm-Sidak, see Table 1).

1267

1245

1246

1247

1248

1249

1250

1251

1252

1253

1254

1255

1256

1257

1258

1259

1260

1261

1262

1263

1264

1265

1269

1270

1271

1272

1273

1274

1275

1276

1277

1278

1279

1280

1281

1282

1283

1284

1285

Figure 6: The burst duration of Gly¹-SIFamide-elicited LPG intrinsic bursting was shorter in the presence of the I_{NaP} blocker riluzole. Ai) Gly¹-SIFamide elicited slow intrinsic bursting in the PTX:PD_{hype} (pdn) isolated condition, monitored with extracellular recordings of the LPG neurons (*lpgn*). Aii) In the same preparation, 5 µM Gly¹-SIFamide with 30 µM riluzole to block I_{Nap} also elicited intrinsic bursts in LPG. The bars above the *Ipgn* (Ai-Aii) recording highlight the duration of the first LPG burst in SIF:PTX:PD_{hype}. Cycle period (B), burst duration (C) and interburst interval (D) in Gly¹-SIFamide plus PTX:PD_{hype} before (SIF Pre) and after (SIF Post) Gly¹-SIFamide plus PTX:PD_{hype} application in riluzole (SIF Riluzole).. Grey bars in graphs represent mean values in each condition (Gly¹-SIFamide:PTX:PD_{hype}, filled circles; Riluzole + Gly¹-SIFamide:PTX:PD_{hype}, purple circles) (B-D, n = 8; *p<0.05, **p<0.01, ***p<0.001; oneway RM ANOVA, Bonferroni post hoc, see Table 1). Ei) Application of 5 µM Gly¹-SIFamide in the PTX:PDon condition enabled periodic escapes from the pyloric rhythm and generation of several LPG slow bursts. Eii) In Gly¹-SIFamide in riluzole (30 µM) in the PTX:PD_{on} condition, LPG failed to escape and generate slow bursts during steadystate. Instead, LPG remained active in pyloric time (*lpgn*), coactive with the PD neurons (pdn). Scale bar in A applies to A and E, all recordings are from the same experiment.

1286

1287

1288

1289

Figure 7: Blocking both I_h and I_{NaP} did not abolish LPG intrinsic bursting. Ai) In the control condition of Gly¹-SIFamide and PTX with the PD neurons held hyperpolarized (SIF:PTX:PD_{hype}) LPG generated intrinsic slow bursting (*Ipgn*). PD neurons remained silent (*pdn*). Aii) In the presence of 5 μM Gly¹-SIFamide with 30 μM riluzole and 5 mM

CsCl to block I_{Nap} and I_h, LPG generated intrinsic bursts with a shorter burst duration and longer interburst interval. Black (burst duration) and gray (interburst interval) bars from (Ai) are replicated for comparison. Scale bars apply to both panels. Recordings are from the same preparation.

1295

1296

1297

1298

1299

1300

1301

1302

1303

1304

1305

1306

1307

1308

1309

1310

1311

1312

1313

1291

1292

1293

1294

Figure 8: In low Ca²⁺ saline, Gly¹-SlFamide-elicited intrinsic bursting progressively weakened, and trough voltage progressively depolarized in the isolated LPG neuron. A) Intracellular recording from an LPG neuron (top trace) in PTX with the PD neurons hyperpolarized (PTX:PDhype; PD neuron bottom trace) in 0.1X [Ca²⁺] saline (equimolar Mn²⁺ substitution). The dashed line indicates the initial trough membrane potential. The onset and development of Gly¹-SIFamide effects are visible across an approximately 400 second window. The small events in PD are ectopic spikes that passively propagate to the somatic recording site. Ectopic spikes can be activated via modulation of secondary spike initiation zones along the axon (129). Gly¹-SIFamide occasionally activates ectopic PD neuron spiking which does not alter LPG activity (Fahoum and Blitz, unpublished). At the arrow, the amount of hyperpolarizing current injected into PD was increased and the unbalanced bridge recording saturated toward the end of the time shown (straight line). Ai) Regions from A (bars and labels: Onset and Steady-State) are shown at an expanded time scale to highlight the changes in bursts between the onset and steady-state of Gly¹-SIFamide effects in low Ca²⁺ saline. Dashed lines mark trough potential levels at onset of Gly¹-SIFamide effects in low Ca²⁺. B) Traces from the respective control application of Gly¹-SIFamide in PTX:PD_{hype} at onset (*left*) and during steady-state (*right*). Dashed lines indicate trough

potential values at onset of Gly¹-SIFamide effects in low Ca²+ PTX for comparison.

Scale bars in B apply to Ai and B. All recordings are from the same preparation.

1316

1317

1318

1319

1320

1321

1322

1323

1324

1325

1326

1327

1328

1329

1330

1331

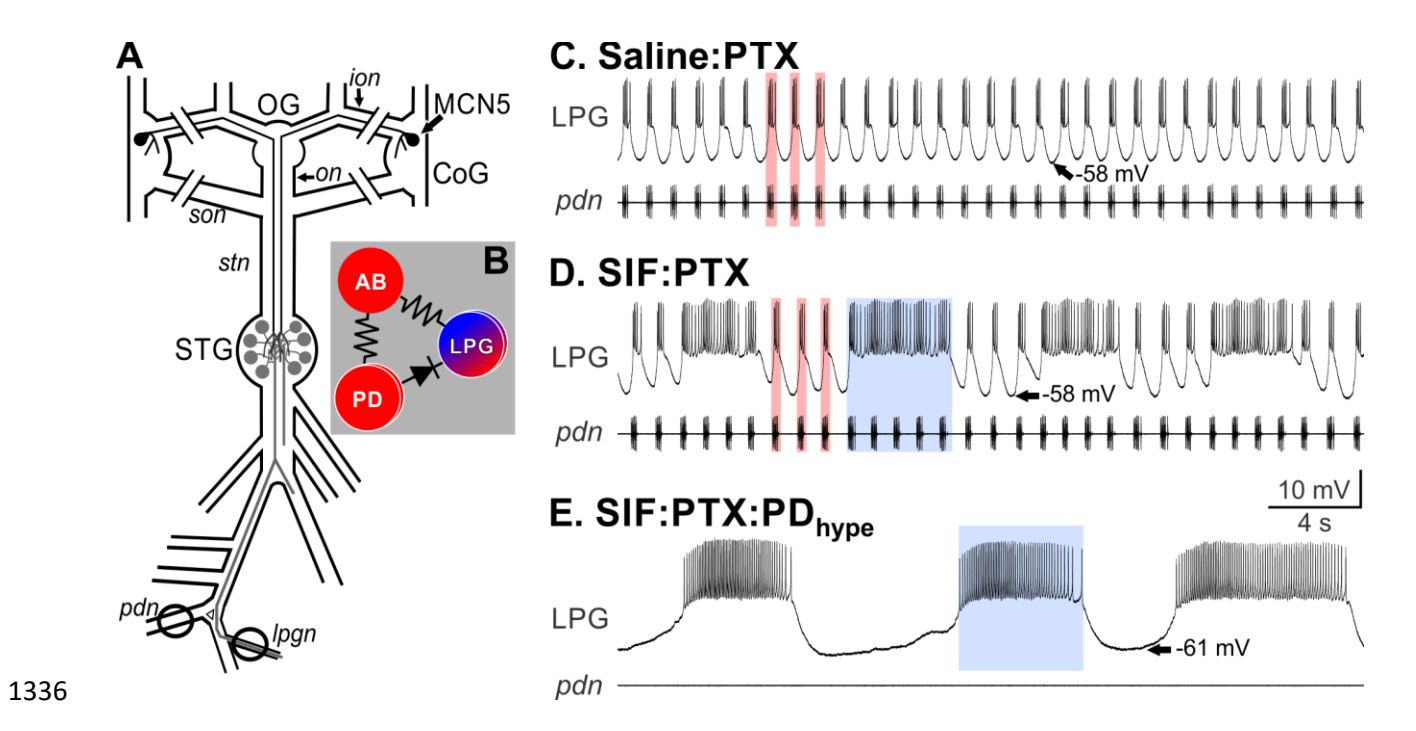
1332

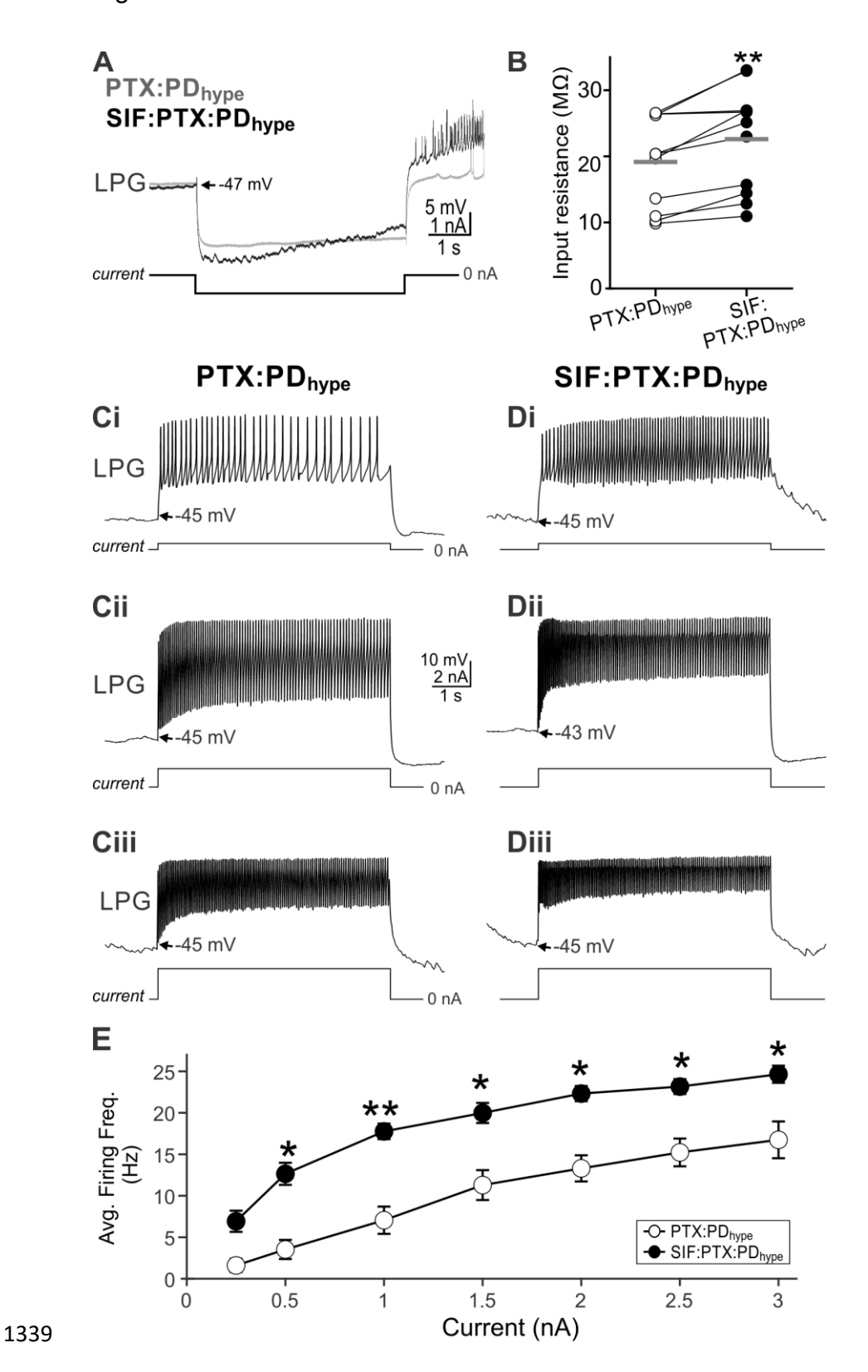
1333

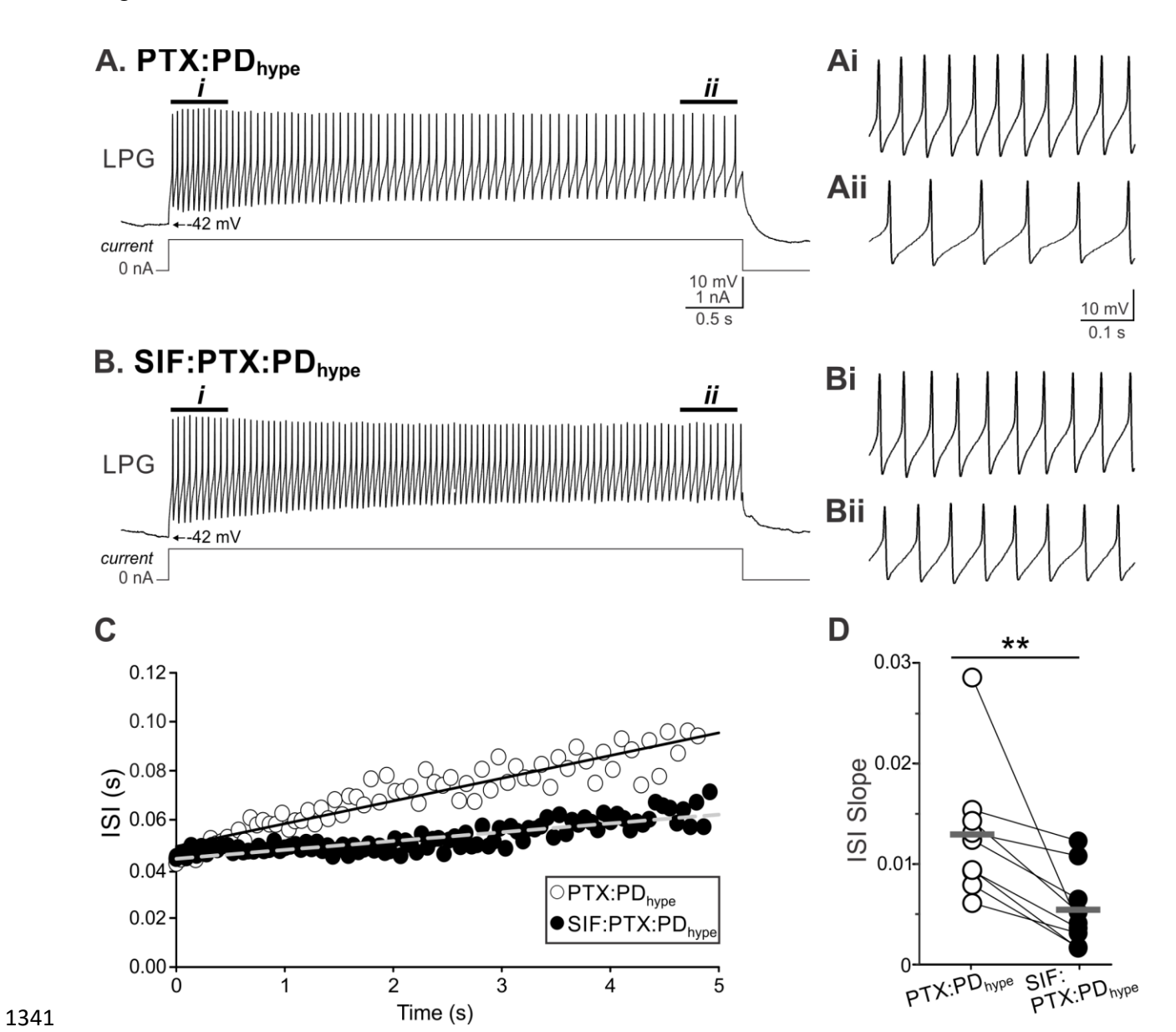
1314

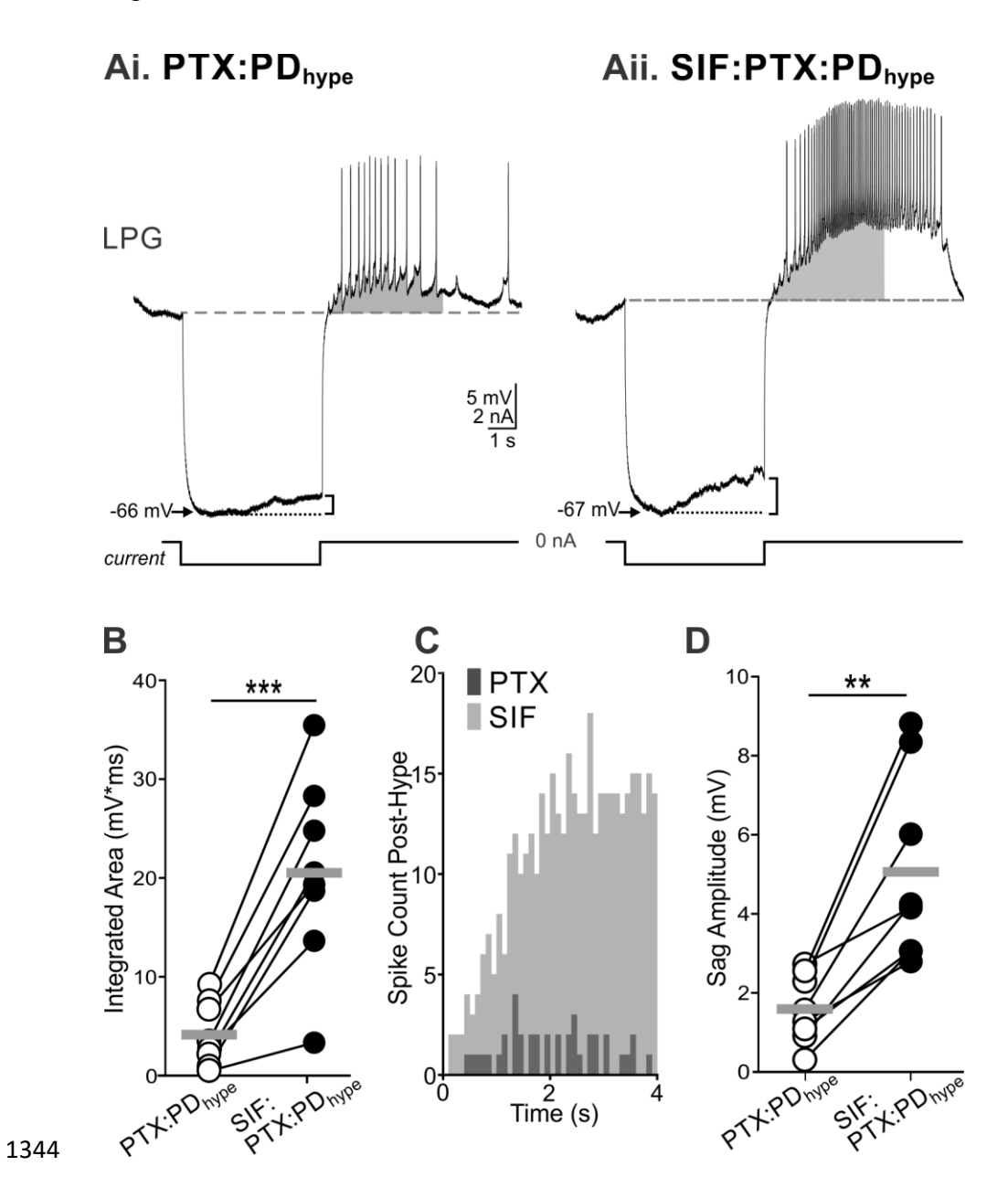
1315

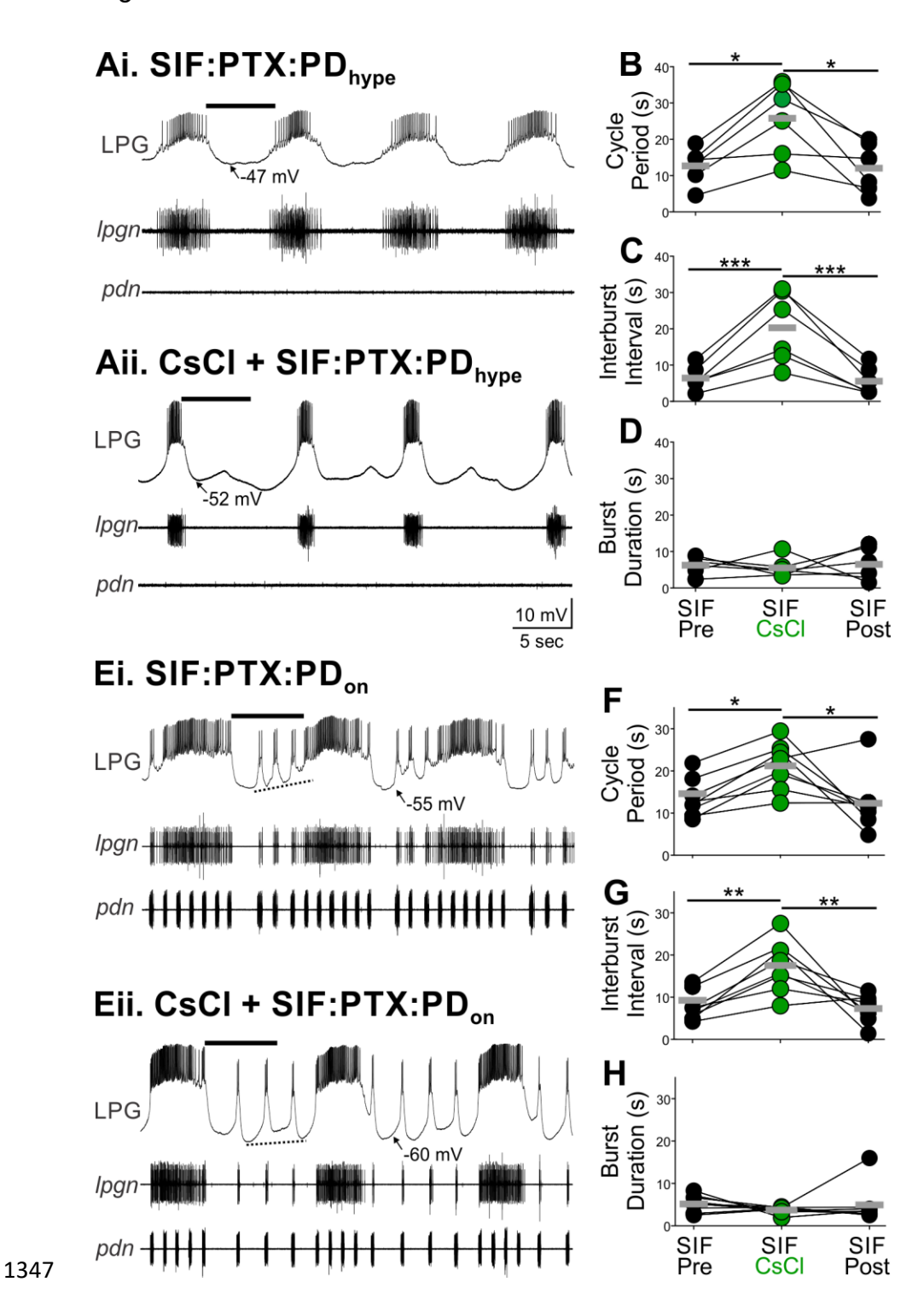
Figure 9: In low Ca²⁺ saline with the pyloric rhythm intact, Gly¹-SlFamide-elicited intrinsic bursting was blocked, and trough voltage progressively depolarized. A) Intracellular recording from an LPG neuron (top trace) in the presence of PTX with the pyloric rhythm intact (PTX:PD_{on}; *pdn* bottom trace) in 0.1X [Ca²⁺] saline (equimolar Mn²⁺ substitution). The black dashed line indicates the initial trough membrane potential. The onset and development of Gly¹-SIFamide effects are evident across a 400 s window. A few extended LPG bursts do occur but coincide with extended PD neuron bursts (red boxes). Ai) In regions from A (bars and labels: Onset and Steady-State) displayed at an expanded time scale, it is evident that LPG only produces pyloric-timed bursting and no slow bursts at onset or steady-state of Gly¹-SIFamide effects in low Ca²⁺ saline when the pyloric rhythm is active. Note the depolarized troughs (Ai, Steady-State) compared to onset bursts (Ai, Onset) and degradation of spike amplitude. The dotted line marks the trough voltages at onset of Gly¹-SIFamide effects in low Ca²⁺ saline. B) Expanded traces from the respective control application of Gly¹-SIFamide in PTX:PDon at onset (left) and during steady-state (right). Dotted lines indicate trough potential values at onset of Gly¹-SIFamide effects in low Ca²⁺ PTX for comparison. Scale bars in Ai apply to Ai and B. All recordings are from the same preparation.

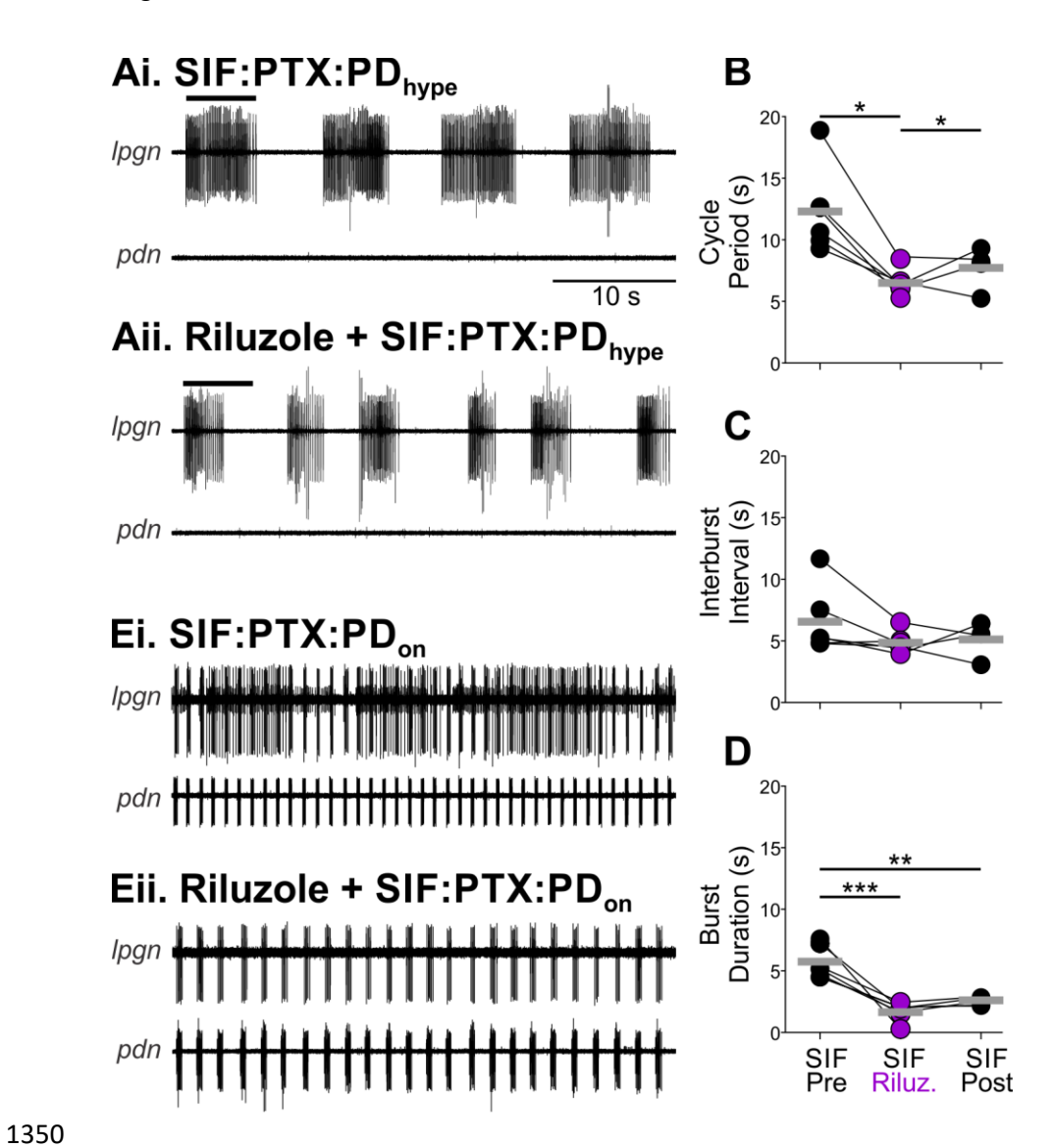


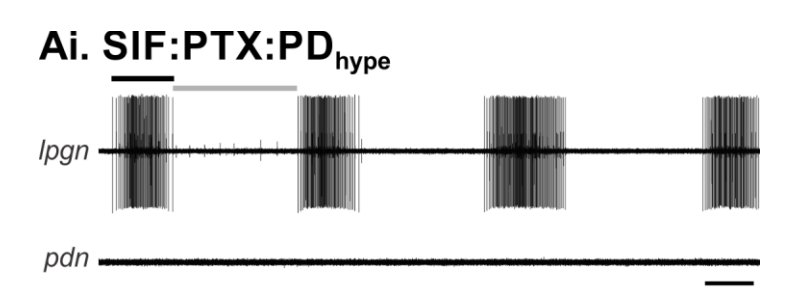


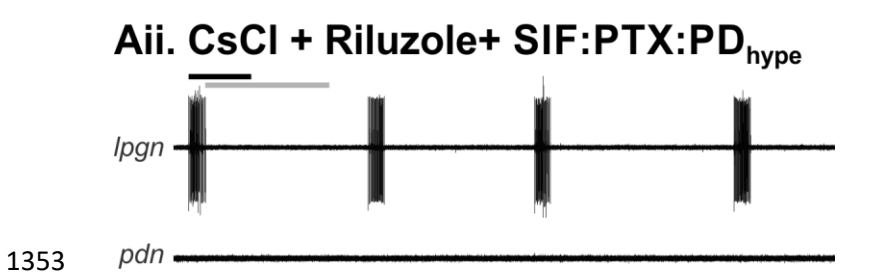








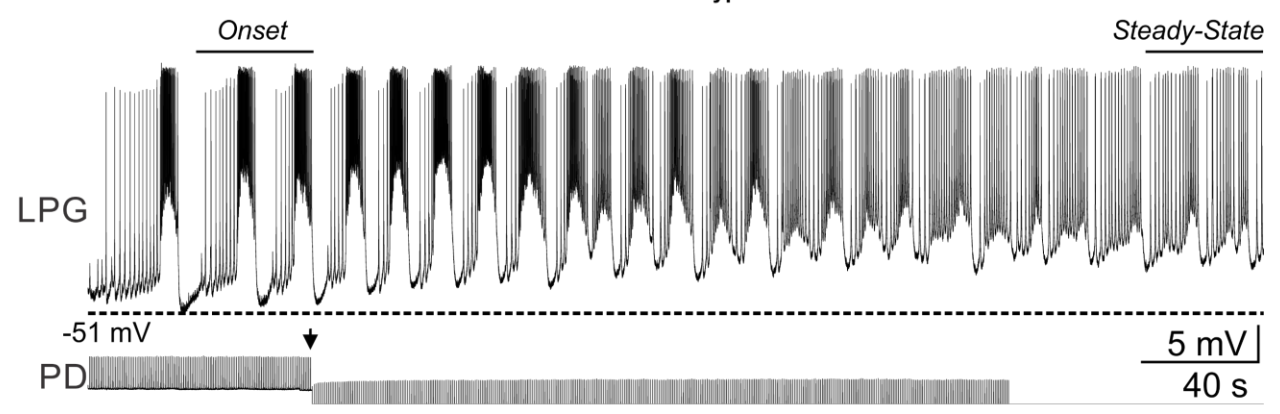




1356

1357

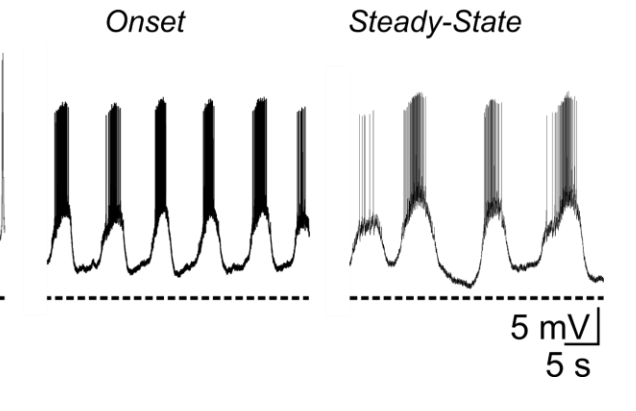
A. Low-Ca²⁺/Mn²⁺ Saline + SIF:PTX:PD_{hype}



Ai. Low-Ca²⁺:SIF:PTX:PD_{hype}

Onset Steady-State LPG -51 mV

B. SIF:PTX:PD_{hype}



1359

-55 mV

A. Low-Ca²⁺/Mn²⁺ Saline + SIF:PTX:PD_{on}

